(p,xn) CROSS-SECTIONS IN 232Th

ру

Ho Chun SUK

A THESIS SUBMITTED TO THE FACULTY OF GRADUATE STUDIES AND RESEARCH OF McGILL UNIVERSITY IN PARTIAL FULFILLMENT FOR THE DEGREE OF MASTER OF SCIENCE.

> Foster Radiation Laboratory Department of Physics McGill University Montreal 110, P.Q., Canada SEPTEMBER, 1971

# TARLE OF COMMENTS

And the second of the second o

				•		
3	•	•		TABLE OF CONTENTS		
. 4		ABSTRACT	• • • • • •		age i	
	:	LIST OF	TABLES .	• • • • • • • • • • • • • • • • • • • •	ii	
	•	LIST OF	FIGURES	••••••	ii	
		CHAPTER	I. INTRO	ODUCTION	1	
		CHAPTER	II. BAC	KGROUND OF THEORY AND PREVIOUS		
	•		EXP	ERIMENTAL RESULTS	4	
			II-1. B	ackground of Theory	4	
			II-2. P	revious Experimental Facts	8	
		CHAPTER	III. EX	PERIMENTAL METHOD	16	
			III-1.	General Method	16	
			III-2.	The Cross-Section	17	
		CHAPTER	IV. EXP	ERIMENTAL ARRANGEMENT AND APPARATUS	22	
			IV-1. P	reparation of Targets and Thickness		
			M	easurements	22	
			. A. G	eneral Physical properties of Thorium	22	
			B. V	acuum Deposition of the Thin Foil		
			Т	arget	22	
			C. M	leasurements of Target Thickness	25	•
		•	IV-2; D	egraded Beam Bombardments Using an		
•		•	A	malyser Box	27	
	•	-	A. I	ntroduction	27	
			В. Т	he External Beam Set-Up	·29	
			C. B	Sombardments and Calibrations	33	
			IV-3. P	Particle Detector and Electronics	38	
_						
Ŧ.				•		

• .

•

# 

REFERENCES.....81

# LIST OF TABLES

Table		Page
4-1.	Physical properties of Thorium-232	. 24
4-2.	Evaporation scheme for thorium targets	. 25
5-1.	(A) Collateral series data of 227Pa	. 45
	(B) Collateral series data of 226 Pa	. 46
5-2.	Experimental $^{232}$ Th(p,6n) $^{227}$ Pa cross-sections	. 52
5-3•	Experimental <sup>232</sup> Th(p,7n) <sup>226</sup> Pa cross-sections	• 53
5-4.	(Information on $(\Gamma_n/\Gamma_T)$ )	. 71
AII-I	l. Half-life data for thorium-232	. 78
AII-2	2. Alpha-energy standards in thorium	• 79
	LIST OF FIGURES	
Figu	re	Pa.ge
4-1.	(A) Surface colours of thin thorium target	
	foils used in this experiment	.23
	(B) Mechanical detail of target	23
4-2.	Plan of the external beam system of the McGill	
	synchrocyclotron	, 28
4-3.	The elements of the bombardment system	, 30
4-4.	Beryllium degrader thickness as a function of	
	degraded proton beam energy with incident beam	
	energy 103.0 MeV	. 31

,	
	Figure
	4-5. Mechanical details of Faraday cup, aluminum window,
	collimator and target holder in the bombardment
	system 32
	4-6. Block diagram of proton charge measurement system 35
	4-7. Measurement of the degraded beam energy by
,	using probability paper
	4-8. A block diagram of the alpha-particle detector
	and analyser system
	4-9. Range-energy curve for alpha-particles in Si 41
	4-10. Mechanical diagram of the detector chamber 42
·	5-0. Nuclide chart for a portion of the heavy region 47
	5-1. The measured excitation functions for the 232Th(p,6n)
	and <sup>232</sup> Th(p,7n) reactions
	5-2. Comparison of $^{232}$ Th(p,6n) $^{227}$ Pa excitation function
	with previous experimental results 57
	5-3. Variation of theoretical excitation function with
	nuclear temperature according to equation (5-4) 62
	5-4. Theoretical <sup>232</sup> Th(p,6n) cross-section normalized
	to the same peak height as the experimental points 63
	5-5. Theoretical <sup>232</sup> Th(p,7n) cross-section normalized to
	the same peak height as the experimental points 64
	5-6. $(\lceil n/\lceil n \rceil)$ as a function of A for fissionable nuclides. 72
Ž	- iii -
<u>.</u> .	

#### CHAPTER I

#### INTRODUCTION

In this laboratory, a number of experiments have been done to measure both relative and absolute nuclear reaction cross-sections, and excitation functions. This thesis describes the modification of a method used for the determination of absolute (p,xn).cross-sections on the natural alpha-emitter thorium-232, which may prove valuable in similar measurements on other naturally active targets as well.

As early as 1956, absolute (p,xn) cross-section measurements were carried out on the heavy element bismuth by Bell et al (1) using the internal circulating beam of the McGill synchrocyclotron. The first measurement of a reaction cross-section using the external proton beam was made in 1964, when Kavanagh et al (2) made a precise determination of the  $^{12}\text{C}(p,pn)^{11}\text{C}$  cross-section at 98 MeV. By degrading the external beam energy with beryllium absorbers, Turcotte (3) in 1968 developed a technique to measure a set of relative (p,xn) cross-sections for  $^{127}\text{I}$ , and in 1970 Chang (4) described measurements of absolute (p,xn) cross-sections in  $^{89}\text{Y}$ . The cross-sections of Turcotte's work (3) were obtained by bombarding the iodine in the form of CI4 and monitoring the production of  $^{11}\text{C}$  for which the cross-sections were well known.

Targets used in the earlier experiments (5,6,7,8,9) were in most cases thicker than those used in the present experiment (about 200-300  $\mu g/cm^2$ ). By a technique to be

described in Chapter IV, two problems (those of determining detector efficiency and of measuring target thickness and uniformity) have been simultaneously solved. The method also makes it unnecessary to measure  $\beta^+$  activity from carbon monitors, a technique which is often difficult because of undesirable activities built up in other (p.xn) reactions.

The bombardment system is arranged so that the degraded external proton beam of the McGill synchrocyclotron passed through thin targets of uniform thickness and was collected in a Faraday cup. Activities produced in the thorium were detected and measured by using a silicon surface barrier detector and multichannel analyser. Yields of a particular (p,xn) reaction were measured by observing the intensity of a suitably chosen known alpha-line in the spectrum from the decay chains of the reaction product. Assuming known branching ratios for the reaction product decay chains leading to the alpha emission chosen, the absolute cross-section for the reaction at the peak of the excitation function could in most cases be determined to an accuracy of better than ±6% including both the systematic error and the constant error due to the half life of the <sup>232</sup>Th(p,6n) reaction. In the worst cases, cross-section errors of the (p,6n) reaction never exceeded about ±15%, including this constant error. In the <sup>232</sup>Th(p,7n) reaction cross-section values, the total error is of the order of ±25%. experimental arrangement and apparatus are described in Chapter IV, and the results are presented in Chapter V.

results are compared with a theory developed by Jackson (10), based on the idea that a (p,xn) reaction cross-section includes both prompt neutron knockout cascades followed by slower neutron evaporation from an excited nucleus. This has been used extensively as a model to study (p,xn) and similar reactions, and the agreement with experiment has been generally satisfactory. The results for the (p,6n) measurements will be compared with those of other workers (6,7,8). The excitation function for the (p,7n) reaction has not been previously measured.

In Appendix I, a sample calculation of the present cross-section values has been made to illustrate the method. Appendix II contains information about the half-life of thorium-232 and its alpha-particle energies, which was used to provide an energy calibration.

#### CHAPTER II

BACKGROUND OF THEORY AND PREVIOUS EXPERIMENTAL RESULTS

## II-1 Background of Theory

Even with the same projectiles and target nuclei, there are several types of reaction, each exhibiting characteristic experimental features, and each corresponding to a different theoretical model. The different reaction types are of varying importance, depending on bombarding energy, the mass of the nuclei involved, and so forth. The general features of the reactions are well described by Blatt and Weisskopf (11) and Preston (12).

In fact, most observed (p,xn) cross-sections have up to now been compared with the statistical theory, with the aim of deriving statistical properties of cross-sections from given models. Thus average cross-sections, auto-correlation functions etc, have been evaluated by many authors using different assumptions.

These calculations amount to evaluating expectation values of products of cross-sections taken at various energies. The description of the reaction mechanisms is usually based on the model of the compound nucleus and evaporation; that is, the two steps of the reaction can be considered as separate processes. The first step is that (incident particle + initial nucleus —> compound

nucleus), and the second step is that (compound nucleus-

In Blatt and Weisskopf's (11) nuclear evaporation model which may correspond to a bombarding energy below 20 or 30 MeV per incident nucleon, the intensity of the spectrum of outgoing particles such as neutrons is given by

$$I_{b}(E_{e}) \propto E_{e} \sigma_{c}(E_{e}) W_{v}(E_{bv} - E_{e})$$
 (2-1)

where  $\sigma_c(E_e)$  is the total cross-section for collision between a neutron of energy  $E_e$  and the excited nucleus (i.e., as through the reaction proceeded in reverse);  $(E_{by} - E_e)$  is represented as an excitation energy which is just equal to the kinetic energy of the captured particle in the centre-of-mass system plus its binding energy in the compound nucleus, and  $W_y(E_{by} - E_e)$  is called the level density. For neutrons, Blatt and Weisskopf(11) have expanded  $\log^W y(E_{by} - E_e)$  around  $E_{by}$  in a Taylor's series:  $\log^W y(E_{by} - E_e) = \log^W y(E_{by}) - E_e(\operatorname{dlogW}_y/\operatorname{dE})_{E=E_{by}} + \cdots$  (2-2) and integrate this to give

$$W_{y}(E_{by} - E_{e}) = \exp(-E_{e}/T)$$
 (2-3)

where  $T = (dlogW_y/dE)$  is defined as the nuclear temperature after the neutron has evaporated. Thus,

$$I_{b}(E_{e}) \propto \sigma_{c}(E_{e}) \exp(-E_{e}/T)$$
 (2-4)

gives the spectrum for the emitted neutrons.

Clearly for a highly excited nucleus a whole chain of such evaporation can be envisaged, and one can calculate such quantities as the average number of neutrons emitted, and the total energy spectrum. These chains have been studied by

Jackson (10) who has particularly paid attention to (p,xn) and, to a much lesser extent, (p,pxn) reactions with incident proton energies up to 100 MeV. Serber (13) also has dealt with incident particle energies of 100 MeV or more, in which the reaction processes are caused by a different mechanism from that of the Jackson model (10).

Jackson (10) has considered the reaction to be divided into two steps: a prompt multiple collision process, followed by an evaporation stage. Then, the first step in calculating a (p,xn) or (p,pxn) reaction cross-section is the determination of the relative probabilities q(i,j) for the ejection of i prompt neutrons and j prompt protons from a heavy nucleus bombarded by protons as a function of the incident proton energy  $E_{\rm O}$  in MeV. In the second step, Jackson (10) assumed that the neutron energy spectrum is  $E_e \exp(-E_e/T)$  and that neutron emission occurs whenever it is energetically possible; he thus calculates the probability that x neutrons are evaporated in a collision with excitation energy  $E^*$ , and calls it  $P(E^*,x)$ . Jackson (10) was then able to express the (p,xn) reaction cross -section by averaging the neutron evaporation probabilities over the various excitation distributions of the pertinent prompt processes and by weighting them with the relative probability for each prompt process:

 $\sigma(p,xn) = \sigma_c(E_0) \sum_{i=0}^{X} q(i,0) < P(E^*,x-i) > \qquad (2-5)$  where  $\sigma_c(E_0)$  is the reaction cross-section caused by an incident proton of energy  $E_0$ ; q(i,0) is the relative probability

of the emission of i prompt neutrons and no prompt protons; and <P(E\*, x-i)> is the averaged neutron evaporation probability for the remaining (x-i) neutrons at a given excitation energy E\*. In Jackson's derivation, the result is calculated as follows:

- a).  $\sigma_{c}(E_{c})$  is taken from Shapiro (14).
- b). The information about the various prompt processes are obtained from the results of a Monte Carlo type calculation (15) based on a succession of quasi-free, two body collisions. In the Monte Carlo type calculation (15), numerical calculations are made for a large number of representative cascades where the states of the interacting collision partners are picked at random out of all possible ones.
- c). Proton evaporation is neglible due to the Coulomb barrier.
- d).  $P(E^*,x) = I(\Delta_X,2x-3) I(\Delta_{X+1},2x-1)$  (2-6) where I(Z,n) is Pearson's incomplete gamma function

$$I(z,n) = (1/n) \int_0^x x^n e^{-x} dx$$
 (2-7)

and  $\Delta_{\mathbf{X}} = (\mathbf{E}^* - \sum_{i=1}^{X})/T$  is the energy (in units of T) above threshold for the emission of x neutrons, where T is the nuclear temperature which can be adjusted in order to obtain the best agreement with experiment.  $B_i$  is the binding energy of the  $i^{th}$  neutron which can be slightly adjusted as well as can the nuclear radius.

e). The resulting (p,xn) cross-sections were compared with the experimental data of Bell and Skarsgard (l).

Experimental data of (p,xn) reaction cross-sections can then be compared with Jackson's statistical model (10) by taking  $\sigma_{\rm C}(E_0)$  from Shapiro (14) or from Blatt and Weisskopf (11), while q(i,j) and P(E\*,x-i) can be estimated from the diagrams of q(i,j) and P(E\*,x) respectively given by Jackson (10). II-2 Previous Experimental Facts

Data have been collected from many studies carried out on isotopes of the medium and lighter elements.

With alpha-particles of energy up to 18 MeV, Bradt and Tendam (16) irradiated stacked foils of silver and rhodium and observed the yield of radioactive isotopes resulting from  $(\alpha,n)$  and  $(\alpha,2n)$  reactions. The energy of the alpha-particles activating a particular foil in the stack is obtained from the known degradation in energy that the incident alpha particles suffer after passing through matter. The cross-sections obtained show the characteristic compound nucleus shape and can be fitted by evaporation theory by assuming a nuclear temperature T=1.8 MeV.

Ghoshal (17) carried out experiments which provide a direct proof of the compound nucleus reaction mechanism. <sup>64</sup>Zn was formed in two different ways by bombarding stacked foils of nickel (<sup>60</sup>Ni) with alpha-particles of energy up to 40 MeV and copper foils (<sup>63</sup>Cu) with protons of energy up to 32 MeV. Absolute yields of the various radioactive isotopes were

determined by counting positrons emitted in their decay. The ratios of the cross-sections in the two sets of reactions were remarkably similar, giving a direct verification of the compound nucleus theory. The same cross-sections have been measured in <sup>63</sup>Cu by Meadows (18) giving results which agree with this concusion.

Otozai et al (19) measured the excitation functions for the reactions induced by protons on \$100\text{Cd}\$, \$111\text{Cd}\$, and \$112\text{Cd}\$ in the energy range from 5 to 37 MeV. The total reaction crosssections agree with the Calculated values based on the diffused surface optical model.

Porile et al (20) measured the excitation functions for a number of (p,xn), (p,pxn), (p,2pxn) and (p,3pxn) reactions of  $^{69}$ Ga and  $^{71}$ Ga with 13 to 56 MeV protons. Values have been obtained for the total reaction cross-section of  $^{69}$ Ga and they are in agreement with continuum theory values for  $r_0$ =1.4 to 1.5fm.

Saha, Porile and Yaffe (21) worked out the excitation functions for the (p,xn); (x=1 to 4) reactions and (p,pxn); (x=1 to 5) reactions of  $^{89}$ Y with 5 to 85 MeV protons using internal beam bombardments with the McGill synchrocyclotron. Also using thin metallic targets of  $^{89}$ Y, Chang (4) measured the absolute cross-sections of (p,4n) and (p,5n) reactions with degraded external beam energies between 49.0 and 67.0 MeV in this cyclotron, obtaining a nuclear temperature of 1.7 MeV for the  $^{89}$ Y(p,5n) reaction.

Similiarly, Sachdev, Porile and Yaffe (22) worked out the excitation functions for the (p,xn);(x=1 to 5), (p,p3n), and (p,2pxn);(x=1,3,4) reactions induced in <sup>88</sup>Sr by protons of energy from 7 to 85 MeV using the McGill internal beam. The experimental results of both Saha et al (21) and Sachdev et al (22) are compared with Monte Carlo calculations using the codes of Chen et al (23) for the evaporation stage. The comparison suggests that the calculations of Chen et al overestimate the extent of compound nucleus contribution at high energies.

Turcotte (3) measured the relative cross-sections of (p,xn);(x=3,5 to 8) reactions in \$127\$I using the external beam of the McGill synchrocyclotron and a Ge(Li) detector. The nuclear temperature T was varied as a parameter for each reaction. The best fit for each reaction varied from 1.4 MeV for the (p,3n) reaction to 1.8 MeV for the (p,8n) reaction, using calculations essentially based on the Jackson model (10).

Measurements made on the medium-and light weight elements are more extensive but of less interest here than reaction studies for heavier elements. Previous measurements of (p,xn) cross-sections in heavy elements have been confined to proton bombardment energies below 32 MeV or above about 70 MeV, and few absolute values are given. Examples for reactions on the heavy elements are as follows:

Kelly (24,25) has measured the  $(\alpha,2n)$  and  $(\alpha,3n)$  cross-section in  $^{209}\text{Bi}$  at energies up to 30 MeV, and the (d,p),

(d,n), (d,2n) and (d,3n) cross-sections with energies up to 19 MeV. John (26) has measured some  $(\alpha, xn)$  cross-sections in the isotopes of lead at energies up to 48 MeV. Also Kelly (24) measured the (p,2n) cross-section in bismuth-209 at bombarding energies between 9 to 32 MeV, and made measurements of the shape of the (p,n) and (p,3n) cross-section curves; qualitatively, these appear characteristic of the shapes expected from compound nucleus theory. As the proton bombardment energy is raised above the threshold for a particular (p,xn) reaction, the crosssection rises rapidly to a peak and then falls almost equally rapidly above the threshold for the next higher reaction (p,(x+1)n). Fits were made using a nuclear radius parameter of r\_=1.43 fm. Andre et al (27,28) have also measured the (p,n) and (p,2n) cross-sections in bismuth-209 for energies ranging up to 10.6 MeV. The stacked foil technique was used and the incident beam was well defined in energy; here the nuclear radius parameter deduced was  $r_0=1.5 \text{ fm}$ . The results were quite different from those of Kelly (24) in this energy region due to straggling effects of the alpha particles. However because of the lower energy of bombardment, the maximum (p,n) cross-section was not reached and the (p,2n) cross-section was obtained only up to energies less than 1 MeV above the threshold. Their paper includes data showing that Kelly's (25) assumed normalization for the (p,n) crosssection is essentially correct.

The first extensive measurements of (p,xn) crosssections were made by Bell (29) on bismuth. Absolute crosssections for the reactions (p,xn); (x=3 to 7) were obtained for proton energies ranging from 20 to 85 MeV. Bismuth foils of about 80 mg/cm<sup>2</sup> thickness were bombarded with the circulating beam of the McGill synchrocyclotron, together with teflon foils to serve as flux monitors using the known  $C^{12}(p,pn)C^{11}$  crosssection. Skarsgard (30) measured the absolute (p,xn) crosssections of 206Pb over the energy range 15 to 65 MeV for x=1 to 7. Thin target and monitor foils were stacked and bombarded by the internal beam of the 100 MeV McGill cyclotron. Based on their previous work (29,30) Bell and Skarsgard (1) describe measurements of cross-sections of (p,xn) reactions in  $^{209}$ Bi,  $^{206}$ Pb,  $^{207}$ Pb, and  $^{208}$ Pb, covering x=3 to 7 in  $^{209}$ Bi, 2 to 6 in  $^{206}$ Pb, 2 to 4 in  $^{207}$ Pb, and 3 to 4 in  $^{208}$ Pb, over a total proton energy range from 12 to 85 MeV, with an absolute accuracy of about 15%. Each excitation function rises above its threshold to a peak whose height is of the order of one barn, and then falls again to a low and fairly constant value. Although the results from x=3 to 7 are consistent with the formation of a compound nucleus including prompt nucleonnucleon knockout, the experimental (p,2n) cross-section appears to be almost double the value predicted. Since (p,xn) reactions are dominant in the energy range 10 to 40 MeV, their sum approximates the total reaction cross-section; the experimental

sum fluctuates around the smooth curve computed for the compound nucleus model using  $r_0$ =1.3 fm. The fluctuations were similar to, but more marked than, those in the total neutron cross-section for heavy elements in the same energy range. A more detailed theoretical discussion of the results is given by Jackson (10).

Hontzeas and Yaffe (31) used radiochemical techniques to determine the absolute excitation functions for 17 nuclides formed as spallation products from the irradiation of vanadium by protons of energies up to 84 MeV. The shape of the excitation functions showed evidence of the contribution of heavy-particle emission in the reactions of the type (p,3pxn), (p,5pxn) and (p,7pxn).

In an attempt to understand nuclear fission in heavy elements, Holub (32) observed charge dispersion in the fission of  $^{232}$ Th, using McGill's internal beam. In this work, measurements were made of the independent and cumulative crosssections of several elements produced in the proton induced fission of  $^{232}$ Th.

McCormick and Cohen (33) worked out the absolute excitation functions for (p, fission) and (p,xn) reactions in  $^{232}$ Th,  $^{235}$ U, and  $^{238}$ U by using radiochemical techniques. Crosssections for (p,xn) reactions in  $^{238}$ U were found to be quite small. The total reaction cross-sections correspond to a nuclear radius of  $(1,55 \pm 0.1)$ A $^{\frac{1}{2}}$  x  $10^{-13}$  cm. This paper dealt

with the determination of the nuclear radius via total reaction cross-sections, and discussed the discrepancy between electro-magnetic and nuclear determination of the nuclear radius.

For the first time, Tewes and James (34) reported that the work on the (p, fission), (p,n), and (p,3n) reactions on thorium indicated that the (p,xn) processes account for much of the total proton cross-section at all energies up to 20 MeV. Tewes measured the absolute cross-section of these reactions with proton energies up to 32 MeV.

Meinke etal(7) determined the excitation functions for the reactions  $^{232}$ Th (p,xn) in x=3 and 6,  $^{232}$ Th (d,xn) in x=4 and 7,  $^{232}$ Th ( $\alpha$ ,pxn) in x=5 and 8,  $^{232}$ Th ( $\alpha$ ,xn) in x=6 and 7, and  $^{238}$ U (p,pxn) in x=5 and 8. In this experiment, stacked foils of 5-mil thorium or uranium metal with varying thickness of copper metal sandwiched between them were bombarded with charged particles with energies as high as 348 MeV for protons, 194 MeV for deuterons, and 388 MeV for helium ions. results are discussed in terms of compound nucleus formation, transparency effects, fission, and other factors in order to arrive at a qualitative picture for the mechanism of high energy nuclear reactions with heavy nuclei. It may be of some interest to make a more quantitative comparison between the observed peaks of the excitation curves for the (p,6n) and (d,7n) reactions and what would be predicted on the basis of the compound nucleus idea. Unfortunately, the energy scale in

the 232(p,6n) excitation function curve was very approximate because of the spread in initial energy of the incident particles and straggling in the stacked foils.

Lefort ct al (6) studied spallation reactions of thorium by chemical isolation of Pa, Th, Ac, and Ra icotopes at the proton energy 150 and 82 MeV, and measured their absolute cross-sections. Specifically the (p,3n) and (p,6n) reaction cross-sections on thorium were measured at various energies between 28 and 150 MeV. Calculations were carried out by assuming a Serber-Jackson model (13,10), and fission-evaporation competition at each step of evaporation was assumed. In this work, the nuclear temperature is given by T=1.9 MeV.

Brun and Simonoff (8) obtained the the excitation functions of the isotopes 227, 228, and 230 of protactium by using (p,xn) reactions with proton energies between 24 and 155 MeV.

In Hussonnois' work (9), the value of the cross-section of  $^{226}$ Pa production by the  $^{232}$ Th(p,7n) reaction for 155 MeV protons, obtained by comparison with  $^{227}$ Pa, is (1 ± 0.3) mb.

In particular the absolute cross-section of the (p,6n) reaction measured by Meinke et al (7), Lefort et al (6), and Brun et al (8) can be compared with the present experiment.

# CHAPTER III

## EXPERIMENTAL METHOD

The method to be described was developed for measuring cross-sections for proton induced reactions in thin targets of known uniform thickness at this laboratory (3,4); this has been modified in order to determine absolute cross-sections for reactions in thin natural radioactive targets of unknown thickness.

#### III-1 General Method

In this work, thorium targets with measured natural radioactive decay rates between 1.0 and 2.0 counts per minute were bombarded in the external proton beam of the McGill synchrocyclotron. This beam, which was degraded from 103.0 MeV with beryllium absorbers, emerged from the beam line through a 50 mg/cm² aluminum window just in front of the target. Inside the beam tube, and immediately in front of the window was a system of aluminum absorbers and a Faraday cup for measuring the beam energy. Bombardments lasted from 2 to 17 minutes with a proton current ranging from 3 to 15 nano-amperes. The beam current was collected in another Faraday cup just behind the target. The total transmitted charge was measured by monitoring the cup with a pico-ammeter whose output was connected to a voltage-to-frequency converter (VFC); this in turn was fed to a scaler.

The radioactive product nuclides formed in the thorium target decayed via alpha-particle emission, or beta emission,

or orbital electron capture. In this experiment, alphaparticles following these events were detected with a system
comprising a silicon surface barrier detector, a charge
sensitive preamplifier, a main amplifier, and a pulse height
analyser.

#### III-2 The Cross-Section

The definition of a nuclear reaction cross-section is based on the simple picture that the probability for the reaction between a nucleus and a flux of impinging particles evenly distributed in space is proportional to the cross-sectional target area presented by the nucleus. More precisely the cross-section is defined by the equation

$$N_{a}^{\bullet} = I N' \sigma X \qquad (3-1)$$

where  $N_a^*$  is the rate of processes of the type considered in the target area struck by the beam (sec<sup>-1</sup>); I is the total particle current per unit time (sec<sup>-1</sup>); N' is the number of atoms per cubic centimetre of target (cm<sup>-3</sup>);  $\sigma$  is the crosssection (cm<sup>2</sup>); X is the target thickness (cm).

The target is considered to be thin enough that the beam intensity does not decrease significantly when passing through it.

The cross-section  $\sigma$  varies with the kinetic energy E and also with the type of incident particle. This function  $\sigma(E)$  is called the excitation function of the nucleus for the particular process and bombarding particle. In the work to be described proton bombardments were carried out at a number

of incident energies, in order to determine excitation functions for the (p,6n) and (p,7n) reactions on thorium-232.

The following equations illustrate the method used to calculate the cross-sections for the reactions studied. The formula defining the cross-section can be used to find the number of the new species produced in the target area struck by the beam. The flux is defined as

$$\emptyset = D V_0 (3-2)$$

where D is the density of incident particles and  $V_{\rm O}$  is their velocity; here it is assumed that the incident beam is normal to the target plane.

If a new nuclide is produced in the reaction, as in the case of a (p,xn) reaction, the rate of production is

$$dN_a/dt = D V_o \sigma N - \lambda N_a \qquad (3-3)$$

when the new nuclear species is radioactive, with a decay constant  $\lambda$ , where  $N_a$  is the number of nuclei per unit area of the new kind produced by the incident proton beam of velocity  $V_o$ ; N is the number of target nuclei per unit area;  $\sigma$  is the particular cross-section leading from the target nucleus to the desired isotope.

In the equation (3-3), the first term on the right side gives the rate of formation of the new radioactive atoms from the target sample; the second term gives the rate of disappearance of the new product because of their radioactive disintegration.

The integral of equation (3-3) is given by

$$N_a(t) = D V_0 \circ N (1 - e^{-\lambda t}) / \lambda$$
 (3-4)

or

$$N_a(t) = (P/St) \sigma N (1-e^{-\lambda t}) / \lambda$$
 (3-5)

where P is the total number of incident particles (in this case, the total number of protons); S is the total reaction area of the target; t is the length of time for the irradiation of the sample.

Equation (3-4) or (3-5) is the basis of the method usually used to determine the activation cross-section of a nuclide if the flux  $\emptyset$  of the incident beam is known, or for determining the flux of the incident beam when the activation cross-section is known.

In an actual experiment, a finite time  $(t_1 - t)$  must elapse between the end of the irradiation period t and the starting time  $t_1$  of the actual counting. Therefore, the total number  $N_a(t_1)$  of the new radioactive atoms per unit area still existing in the target at time  $t_1$  is

$$N_a(t_1) = (P/St) (\sigma N/\lambda) (1 - e^{-\lambda t}) e^{-\lambda (t_1 - t)}$$
 (3-6)

Likewise, the number  $N_a(t_2)$  per unit area of the new radioactive atoms still existing in the target at time  $t_2$  when counting stops is

$$N_a(t_2) = (P/St) (\sigma N/\lambda) (1 - e^{-\lambda t}) e^{-\lambda (t_2 - t)}$$
 (3-7)

Therefore, the number of counts recorded by the counting system will be

$$N_a(t_1, t_2) = [N_a(t_1) - N_a(t_2)] \times Y Z$$
  
=  $(P/St)(\sigma N/\lambda)(1-e^{-\lambda t})e^{\lambda t}(e^{-\lambda t}1-e^{-\lambda t}2)XYZ$  (3-8)

where X is the solid angle efficiency of the detector;
Y is the ratio of live time to real time for the analyser;
Z is the fraction of the decays which result in the specific alpha-ray observed. It is assumed here that the counting rate efficiency of silicon detectors for alpha-particles is essentially 100% for any case where the energy lost in the sensitive region gives pulses much larger than the noise level.

Now, the natural decay rate from a radioactive target such as thorium will be

$$(dN/dt)_n = \lambda_n N (3-9)$$

where dN is the total number of atoms per unit area decaying during a time dt. Also, in an actual measurement, the number of decays counted can be expressed by

$$(dN_n/dt)_c = (dN/dt)_n X' Y' Z'$$
  
=  $(\lambda_n N) X' Y' Z'$  (3-10)

and then the number of nuclei per unit area counted is given by

$$N = (dN_{p}/dt)_{c} (\lambda_{p} X' Y' Z')^{-1}$$
(3-11)

where  $dN_n$  is the total number of decays per unit area during time dt; X' is the solid angle efficiency of the detector from the natural source; Y' is the ratio of live time to real time for the anlyser system; Z' is the fraction of the decays which result in the particular alpha-ray observed from the thin foil thorium target.

Substituting equation (3-11) into equation (3-8) gives

$$N_{a}(t_{1},t_{2}) = \frac{P \circ X Y Z}{ST \lambda_{n} X' Y' Z'} (dN_{n}/dt)_{c} (1-e^{-\lambda t}) e^{\lambda t} (e^{-\lambda t_{1}} - e^{-\lambda t_{2}})$$
(3-12)

If the same detector is used to count both natural and induced activity, then S=S', and X=X'. A multiplication of both sides of equation (3-12) by S will then give the total number of recorded counts  $R_a$  from induced radioactivity in area S terms of the counts from natural activity as follows:

$$R_{a}(t_{1},t_{2}) = \frac{PQOYZ}{St\lambda\lambda_{\gamma}Y'Z'} (1-e^{-\lambda t})e^{\lambda t}(e^{-\lambda t}1 - e^{-\lambda t}2)$$
(3-13)

where  $Q=(dN_n/dt)_cS$ . Then the cross-section for the given reaction can be expressed by

$$\sigma = \frac{\text{S t } \lambda_n \text{ Y' Z' } R_a}{\text{P Q Y Z } (1-e^{-\lambda t}) \text{ } e^{\lambda t} \text{ } (e^{-\lambda t}1 - e^{-\lambda t}2)}$$
(3-14)

In effect the use of the same detector in the measurement of induced and natural activity eliminates the problems of directly measuring target thickness and solid angle efficiency.

In the equation (3-14),  $R_a(t_1,t_2)$  and Q are observed by the pulse height analyser; P is given by the measurement of the incident beam charge delivered; Y and Y are determined by calculating the ratio of live time to their counting real time; Z, Z',  $\lambda$ , and  $\lambda_n$  are taken from the known decay schemes of the radioactive nuclide involved. A sample calculation including an estimate of error is given in Appendix I.

#### CHAPTER IV

#### EXPERIMENTAL ARRANGEMENT AND APPARATUS

- IV-1 Preparation of Targets and Thickness Measurements
  - . A. General Physical Properties of Thorium (35)

Thorium occurs in thorite (ThSO4) and in thorianite  $(ThO_2+UO_2)$ . Thorium is now thought to be about three times as abundant as uranium and about as abundant as lead or molybdenum. The metal is fissionable and is a source of nuclear power. Thorium is recovered commercially from the mineral monazite which contains from 3 to 9% Th02 along with most rare-earth minerals. When pure, thorium is a silvery white metal which is air stable and retains its lustre for several months. When contaminated with the oxide, thorium slowly tarnishes in air becoming coloured (see Fig. 4-1(A)), gray and finally black. The physical properties of thorium are greatly influenced by the degree of contamination with the oxide. For this reason, values for the melting point and specific gravity are still in question. The general physical properties of thorium-232 are given in Table 4-1 and its radioactive characteristics are outlined in Appendix II. In this experiment, powdered alpha inorganic thorium was purchased from Ventron (Berverly, Mass., U.S.A.).

B. Vacuum Deposition of the Thin Foil Target

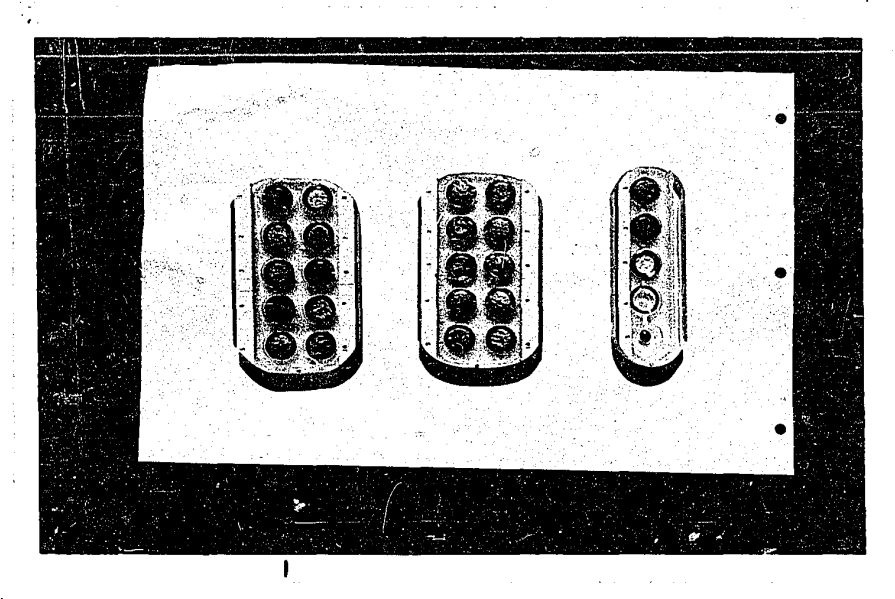
The thorium was evaporated on an aluminum backing

foil of thickness 0.00075 mm. and the foil was then glued to

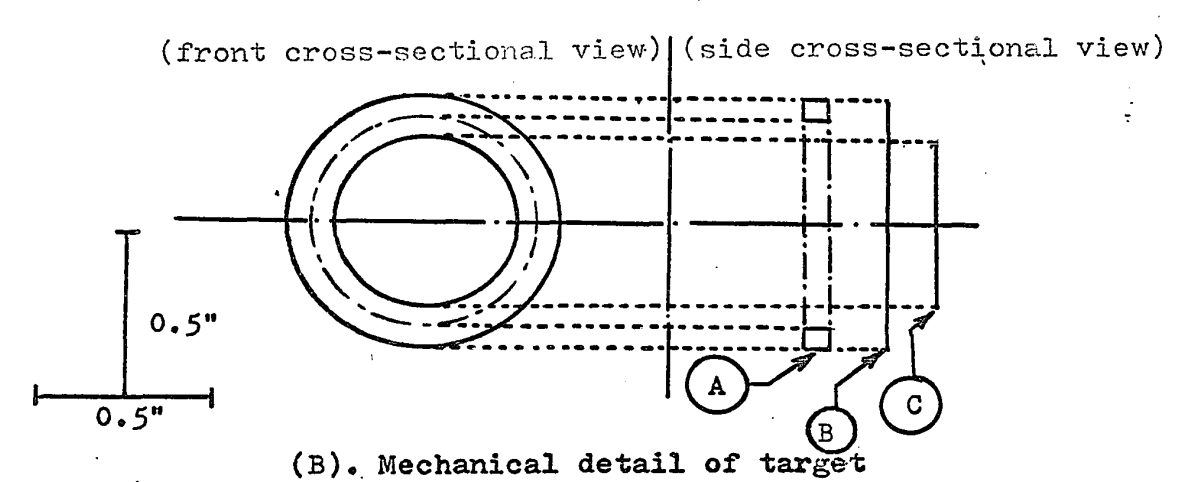
Fig. 4-1

to the second

Fig. 4-1



(A). Surface colours of thin thorium target foils used in this experiment.



A. Mechanical detail of target mounting ring.

(B). Aluminum backing foil ------thickness 0.00075 mm.

(C). The thorium deposited by evaporation.

Table 4-1. Physical Properties of Thorium-232(35)

Atomic weight	232.08				
Atomic number	90				
Valence	Ц				
Crystalline form	Gray, cubic radioactive				
Specific gravity 2 11.66					
Melting Point °C					
Boiling point °C					
Solubility, in gram per 100 cc	Soluble: HCl, H <sub>2</sub> SO <sub>4</sub> , Aqua Slightly soluble: HNO <sub>3</sub>				
· ·					

an aluminum mounting ring (see Fig. 4-1(B)), with a small quantity of vacuum grease.

The vacuum evaporator used contains a Varian e-gun electron beam evaporation source (36). The gun's heating element is a tungsten wire filament mounted to one side of a crucible; this is heated by means of one variac-controlled transformer to give the required electron emission and the electron beam is moved by adjusting a magnetic field with the other variac-controlled transformer to the striking area desired.

A small quantity of powdered thorium was placed in the crucible beneath the mounted aluminum backing foils, and this was heated by the beam until evaporation occurred. The

Table 4-2. Evaporation scheme for thorium targets

technical details of the evaporation scheme are outlined in Table 4-2. An estimate of the evaporated foil thickness was made by weighing foils following evaporation.

Because of the fragility of the foils, the system was allowed to return to atmospheric pressure over a period of about one hour. It was found that if the thorium layer was thinner than about 300 µg/cm², its surface colour began to change due to oxidation in air. The deposited thorium targets were therefore kept in a vacuum of about  $30 \times 10^{-3}$  Torr to preserve them as well as possible. This precaution was probably unnecessary since the oxide does not interfere significantly with the alpha-ray measurements of this experiment.

C. Measurements of Target Thickness
Methods of measuring target thickness are available

whereby the mean thickness of a material may be determined but, with the possible exception of weighing, these involve expensive equipment. In some cases, the thickness may be measured by using optical methods based on a Michelson interferometer. Also, considerable work (37,38,39,40,41,42) has been reported dealing with thickness measurements of thin foils and films based on the absorption or scattering of alpha, or beta particles in matter. In addition, the foil thickness of target material can often be monitored during the evaporation process (43).

In this experiment, the basic method used in the determination of the number of target atoms has been described in Chapter III. Equation (3-11) gives the number of nuclei per unit area bombarded (and counted) in terms of the natural decay count rate, the natural decay probability, and parameters associated with the specific detection system used. Equation (3-14) then gives the value of the cross-section.

In this experiment, the area was equal to S=S'=1.057 cm<sup>2</sup>; the ratio of live time to real time for the analyser could be taken as Y=Y'=100% because of the low decay rate of the natural and induced radioactivity; the fraction of the decays resulting in the alpha-ray observed and the decay constant were taken as Z'=100% and  $\lambda_n$ = 9.413 x 10<sup>-17</sup>/min. respectively by using the known data (see Appendix II): the counting periods for the natural activity of the targets were between

28 and 30 hours, since the observed decay rates were between 1.0 and 2.0 per minute. This counting technique should be useful for cross-section measurements on any naturally radio-active target material (e.g., lutetium, radium, actinium, protactinium, and uranium).

IV-2 Degraded Beam Bombardments Using an Analyser Box

#### A. Introduction

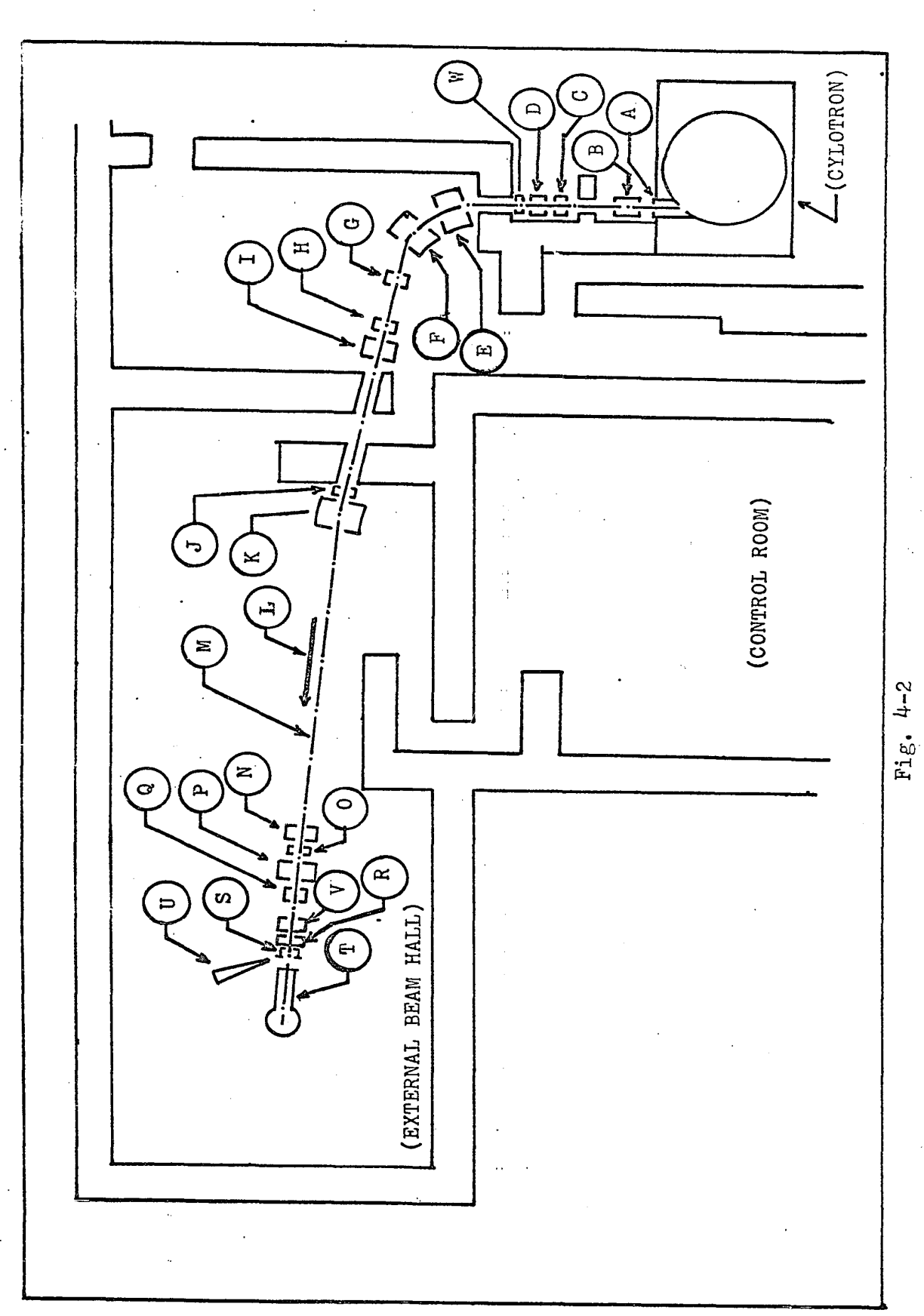
A target holder and Faraday cup were installed in the external beam hall of the McGill synchrocyclotron, and a flexible experimental control and analysis system was assembled for this experiment. A plan of the beam hall, showing the location of this apparatus, is given in Fig. 4-2.

The external beam was used for these activations. The system used in this work was designed for ease in measuring activation cross-sections directly without requiring a known monitor reaction to deduce the bombardment intensity. The inherent advantages of an external beam are its well defined energy and the certainty that the beam passes through the target only once. The current, and total charge through the target can easily be measured in a Faraday cup. In the internal cyclotron beam, the radial oscillations and the precession of the orbits in the median plane of the field cause a significant spread in the energy of bombardment at any given radius and cause many protons to undergo multiple traversals of the target.

# Fig. 4-2

Plan of the external beam system of the McGill synchrocyclotron. The labelled components are identified as follows:

- A = Exit port
- B = Faraday cup (removable)
- C = View box
- D = Slit system
- E & F = Bending magnets
- G = Degrader box
- H & I = 4" and 6" quadrupole magnets
- J = Television view box
- K = Switching magnet
- L = Beam direction
- M = Beam line
- N = Faraday cup
- 0 = Television view box
- P & Q = 6" and 4" quadrupole magnets
- R = Faraday cup with aluminum window
- S = Collimator and target holder
- T = Faraday cup
- U = T. V. camera
- V = Analyser box
- W = Faraday cup



The method and technique of irradiating targets were based on investigations of beam properties in 1971 by Moore (44). Other descriptions of the main apparatus have been given by Turcotte (3), and Chang (4).

# B. The External Beam Set-Up

As shown in Fig. 4-2, the analyser box V is attached to the end of the beam pipe. The details of the bombardment system are presented in Fig. 4-3.

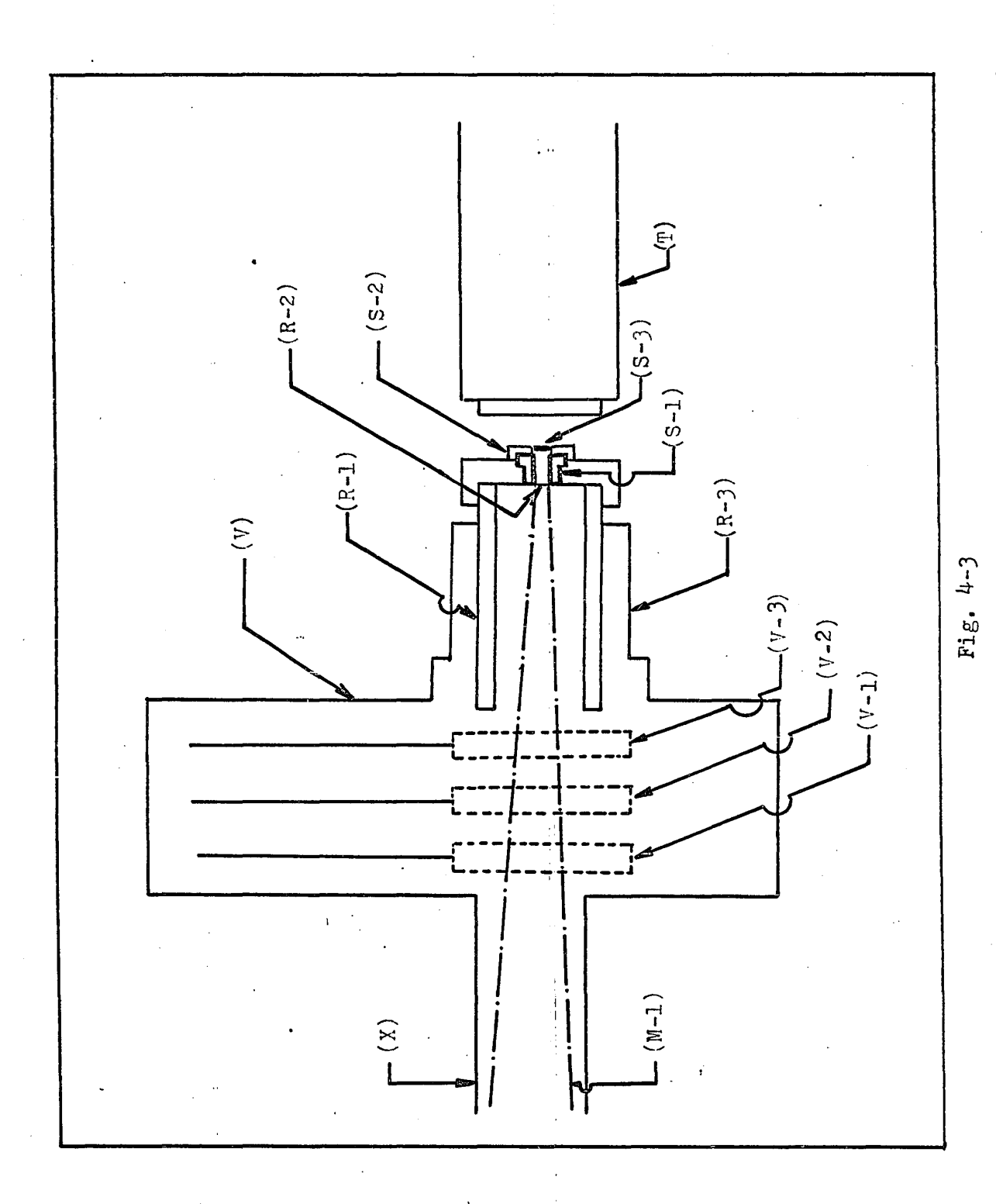
When a specific energy was required, the incident proton beam was degraded by beryllium absorbers. The energy of the transmitted beam as a function of the total thickness could be estimated from Fig. 4-4. These absorbers were installed in the degrader box G of Fig. 4-2. The position of the beryllium degraders was about 10 meters upstream from the target system, at a point where the beam is focused to a small diameter. The beam, which diverges downstream from these absorbers was collimated by the magnetic quadrupole lenses H and I, bent by a switching magnet K, and finally refocused by another quadrupole pair P and Q (see Fig. 4-2). These magnets P and Q are located in front of the bombardment system so as to have a diameter less than 1.2 cm at the target.

The target holder designed for this set of experiments is shown in the detail drawing of Fig. 4-5. For viewing of the beam a scirtillation screen is attached to the aluminum window R-2, and observed by a remote controlled T. V. camera

The elements of the bombardment system

The chamber shown was designed specifically to bombard targets of uniform thickness by a well defined proton beam. The focussed beam passes through the chamber V, containing three wheels with apertures on which are mounted various thicknesses of aluminum (one aperture being vacant). The beam passing through the aluminum is intercepted in the Faraday cup R-1 (a plug is inserted in the beam collimating hole S-1 so that no proton charge escapes from the Faraday cup). The various thicknesses of aluminum are then rotated into the beam to give a range-energy analysis of the protons. Once the energy of the beam has been determined, the plug in the collimator is removed (leaving a 50 mg/cm² aluminum vacuum window between the Faraday cup and the collimator), and the target is bombarded. The beam passing through the collimator onto the target is collected in the Faraday cup.

R-3 = Beam pipe (brass)



- 30-1 -

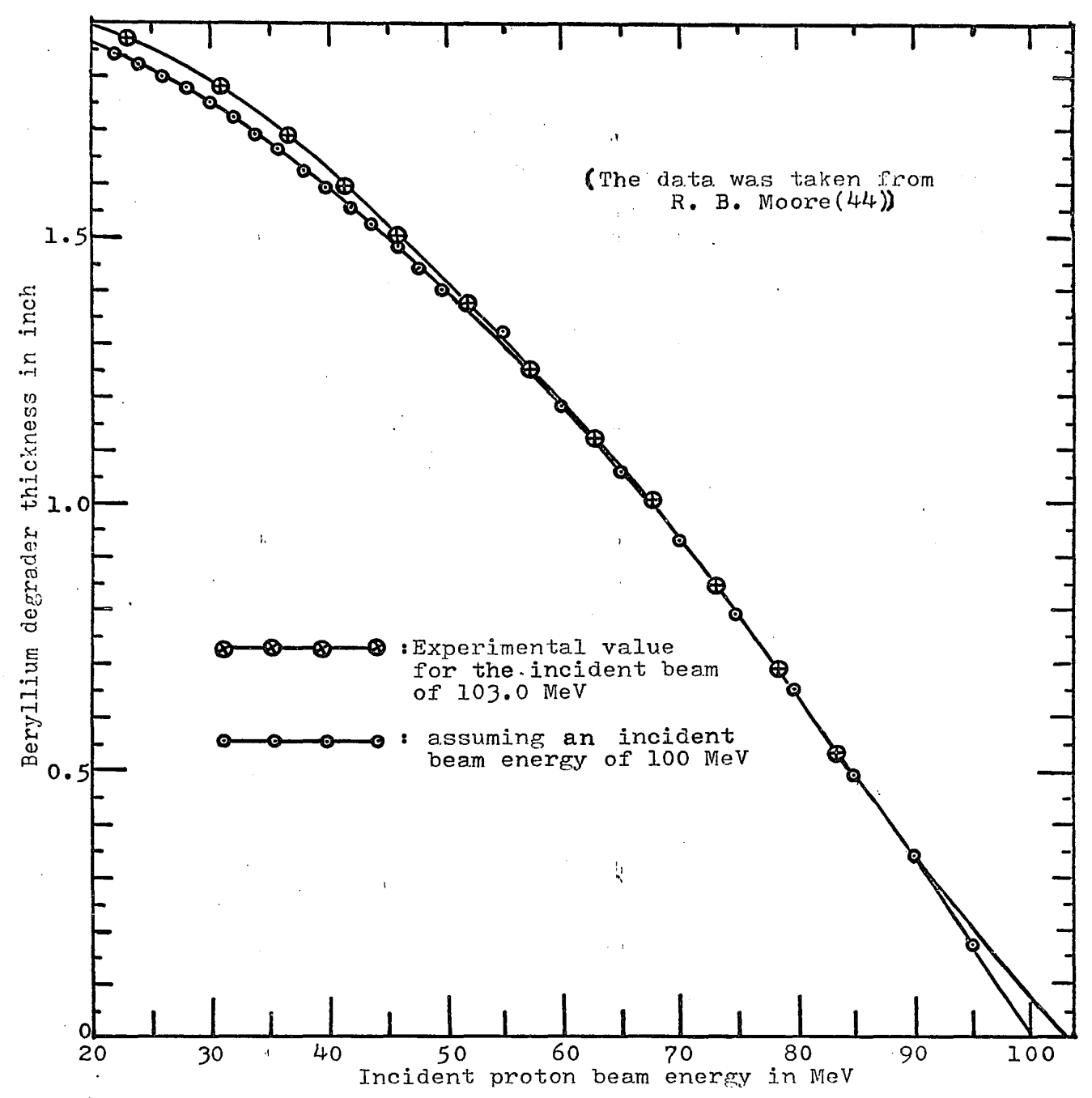


Fig. 4-4, Beryllium degrader thickness as a function of degraded proton beam energy with incident beam energy 103.0 MeV.

## Fig. 4-5

Mechanical details of Faraday cup, aluminum window, collimator and target holder in the bombardment system.

R-1 = Faraday cup (brass)

R-2 = vacuum window of thickness 50 mg/cm<sup>2</sup>

R-3 = beam pipe (brass)

R-4 = aluminum ring with window

R-5 = aluminum ring

R-6 = insulator

R-7 = flange bolt

R-8 = BNC connector

R-9 = 0-ring

R-10 = wire from Faraday cup

S-1 = beam collimator of diamator 1.16 cm

S-2 = target holder

S-3 = target

Fig. 4-5

U (see Fig. 4-3 or Fig. 4-5).

Once the beam has been focused, 1) the scintillator is removed, 2) Faraday cup T (see Fig. 4-2 or Fig. 4-3) was connected to an electrometer via a cable to the cyclotron control 3) The beam collimator S-1 was attached to the window R-2 as shown in Fig. 4-5 and the currents in the quadrupole pairs were adjusted to obtain the maximum transmission of the beam through the collimator S-4 into our standard laboratory Faraday cup T (see Fig. 4-3). The Faraday cup T.was placed as close as possible to the collimator S-1 to minimize the loss of any protons scattered from the window, the target or the air path between the window and the standard cup T. By placing collimating rings around the entrance of the Faraday cup, it was established that 99.0% of the transmitted beam was within a 2" diameter circle at the 4" diameter entrance of the standard cup T. As a further check, the decrease in Faraday cup current for the same cyclotron beam with target out and target in was less than 1.0%. the target was by far the most massive scatterer in the beam path, this indicated that scattering errors were insignificant.

The external beam system was then ready for a bombardment. In this experiment, the details of controlling and setting up the whole beam system were done by co-workers Dr. R. B. Moore and Dr. J. E. Crawford, and the author.

C. Bombardments and Calibrations

After it had been established that a degraded beam of

sufficient intensity was passing through the collimator into the standard Faraday cup, 1) the target holder with target was inserted in the collimator S-1 shown in Fig. 4-5. 2) A current integrator was set up by connecting the voltage output from the electrometer to a voltage-to-frequency converter, which in turn was connected to a scaler. 3) The beam and the scaler were turned on at the same time and the target was irradiated. 4) When the beam was turned off, the irradiation time was noted, as was the final number of counts recorded by the scaler. The digital electrometer used (Keithley Model 615) in conjunction with the VFC (see Fig. 4-6) were accurate to better than 2%.

Immediately after the bombardment, the target was taken to the alpha detector system, and the current integrator was calibrated by using a standard current source set to give a current similiar to the output of the standard laboratory Faraday cup T in the bombarding period. The degraded beam energy was accurately measured by using the analyser box shown in Fig. 4-3, in the following way.

Immediately after obtaining the information for the calibration of the number of protons delivered to the target by using the current integrator, 1) the plug was inserted from the standard laboratory Faraday cup T to a connector on the beam collimator forming a new Faraday cup R-1 (see Fig. 4-3).

2) The T. V. camera was moved to observe the position of the

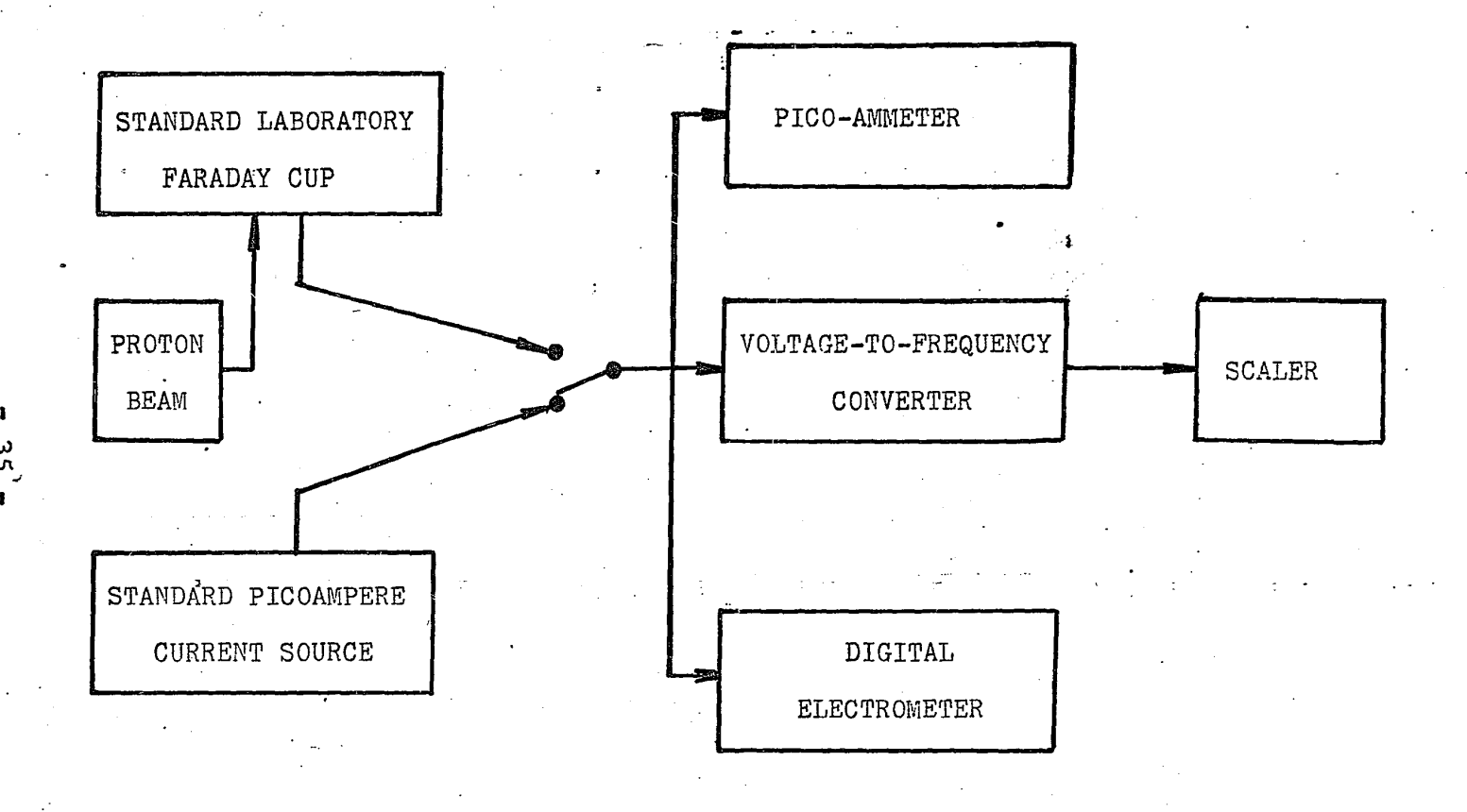
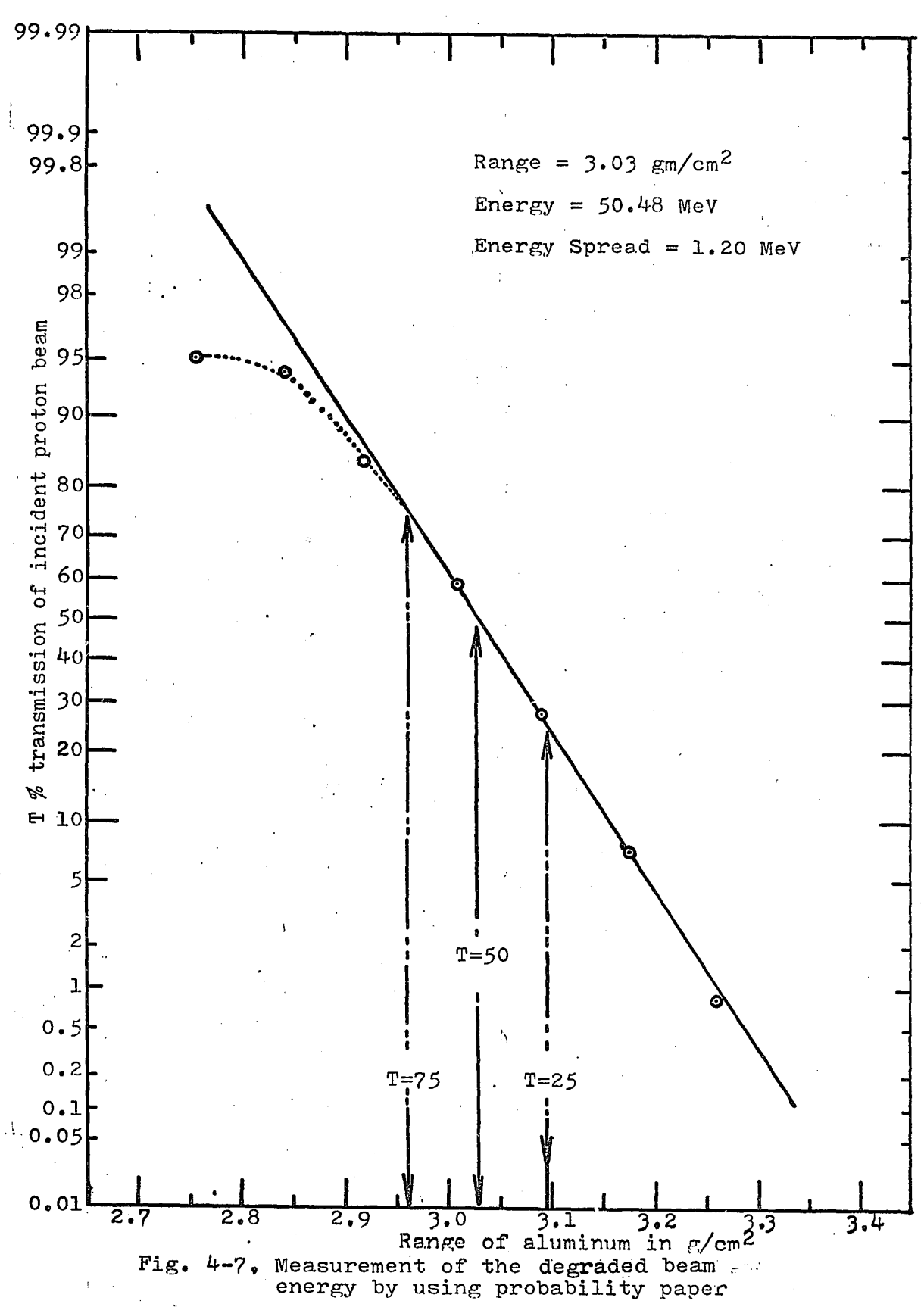


Fig.4-6 Block diagram of proton charge measurement system

analyser wheels. This arrangement allows a convenient and accurate measurement to be made of both the degraded beam energy and its energy spread by observation of the transmission as a function of the aluminum absorber thickness. Interposing successively greater thicknesses of aluminum in the beam eventually stops all transmission.

Theory and experiment show that if a nearly monochromatic beam of protons, with a Gaussian energy spread and fixed intensity are allowed to pass through successively greater thicknesses of an absorber, such as aluminum, then a plot of transmitted beam vs. absorber thickness yields a curve which is the integral of a Gaussian distribution. therefore, if the transmitted current values are properly normalized and plotted on probability paper, a straight line will result. The thickness of aluminum corresponding to a 50% transmission (T=50) is the range of the degraded beam. Two other points are important as well. These are the thicknesses of aluminum corresponding to 25% and 75% transmission (T=25 and T=75), which represent the FWHM of the range of the degraded beam on the probability paper. The energy of the beam and its FWHM are then determined from the empirical tables of range-energy and stopping-power (45).

As can be seen in Fig. 4-7 as an example, the actual transmission as a function of range is not strictly the integral of a Gaussian distribution particularly in the region of less than T=50 thickness. This happens because nucleon interactions have produced a "soft" or low energy component to the beam passing through the aluminum which is removed before the range of the remainder of the beam has been reached. The statistical analysis



which gives the Gaussian integral for the beam transmission and which provides the basis for the range-energy relationship is based on the protons undergoing only low energy transfer collisions with the target's electrons. Almost all of the beam which is transmitted through a thickness greater than T=50 is formed of such protons. Consequently it is this part of the transmission plot which would give the most accurate determination of the energy of the beam entering the aluminum. Under these conditions, however, the low intensity beam leaving the aluminum is widely diverging. Therefore in this design care was taken to place the final aluminum absorber as close as possible to the mouth of the Faraday cup. This allowed easy and accurate measurements of the beam current at transmissions as low as 0.1%.

Thus, information for both the number of protons delivered to the target and the degraded beam energy could be completed in less than 5 minutes after a bombardment.

#### IV-3 Particle Detector and Electronics

In this experiment, the alpha-particle detection and analysis system is represented in Fig. 4-8. A silicon surface barrier detector within an aluminum chamber produced pulses which were fed into a system consisting of a preamplifier and main amplifier; then the amplified pulses were fed into a 20 MHz TMC multichannel analyser system. The analyser output was recorded on magnetic tape for later analysis, or was

read out by a channel printer.

The conventional silicon surface barrier detector used in this experiment is a large area diode consisting of an extremely thin p-type layer on the sensitive face of a high purity, n-type silicon wafer. The two electrical contacts to this diode are made(46): (a) to the p-type surface through a thin gold film approximately 40 microgram/cm<sup>2</sup> thick, and (b) through a non-rectifying metal contact to the n-type silicon on the back surface. In this experiment an Ortec model A-035-050-300 silicon surface barrier detector was used for the detection of alpha-particles. The sensitive depth of this particular detector is 300 microns, with a detector bias of 95 volts. The range vs. energy curve of Fig. 4-9 shows that this is sufficient to stop alpha particles with energy lower than 25 MeV, and is therefore adequate for observing any alpha activity produced.

The detector was enclosed in the cylindrical chamber shown in Fig. 4-10. The chamber was connected to a mechanical vacuum pump with two valves for vacuum isolation and air inlet, and to a vacuum gauge. The vacuum in the system could be reduced to about 30 x  $10^{-3}$  Torr within 30 seconds and  $10 \times 10^{-3}$  Torr within 3 minutes from atmospheric pressure. Within the chamber a ring type of brass collimator (thickness = 0.127 mm, inside diameter = 1.16 cm, outside diameter = 2.0 cm) was designed specifically to define the solid angle of

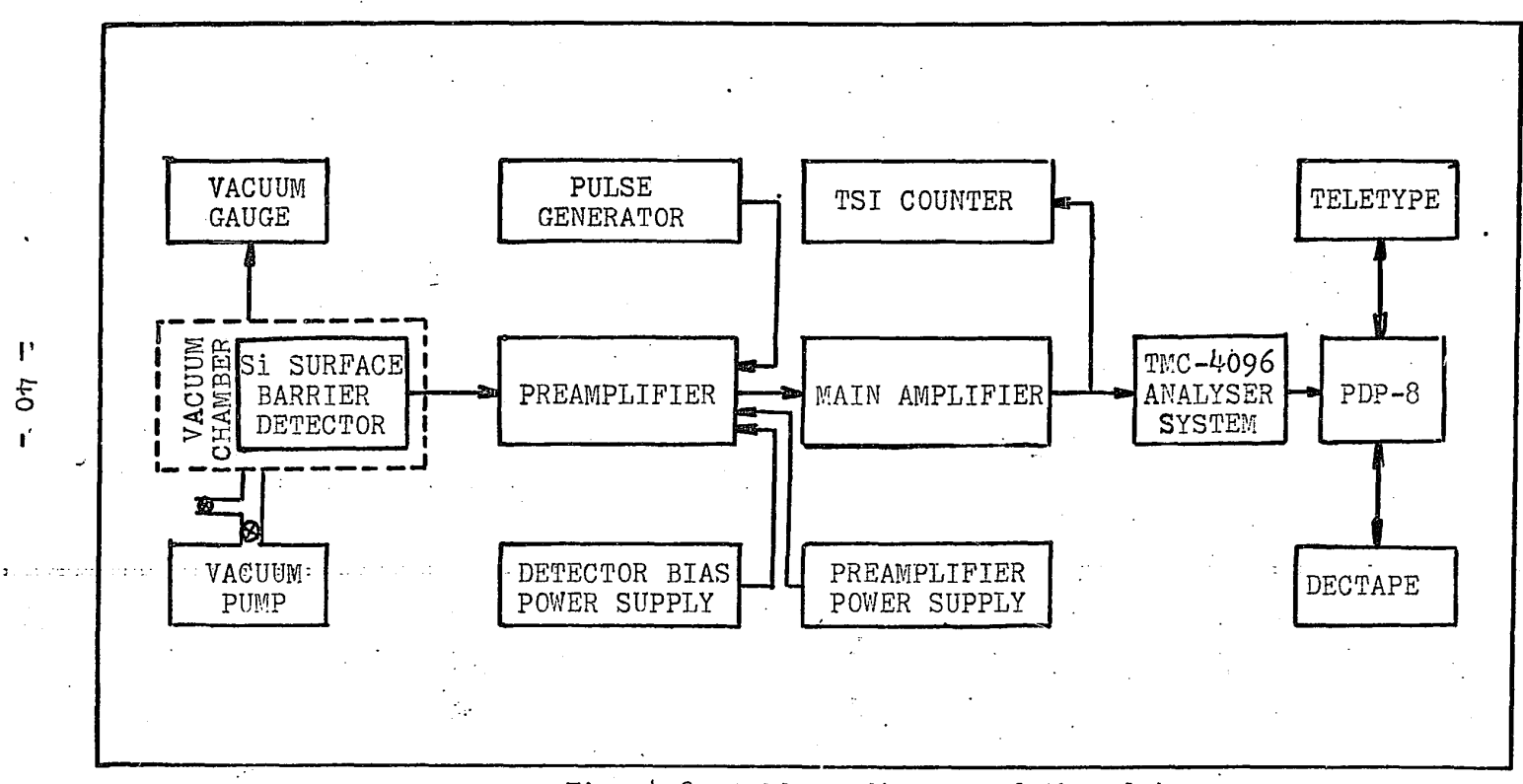


Fig. 4-8 A block diagram of the alphaparticle detector and analyser system

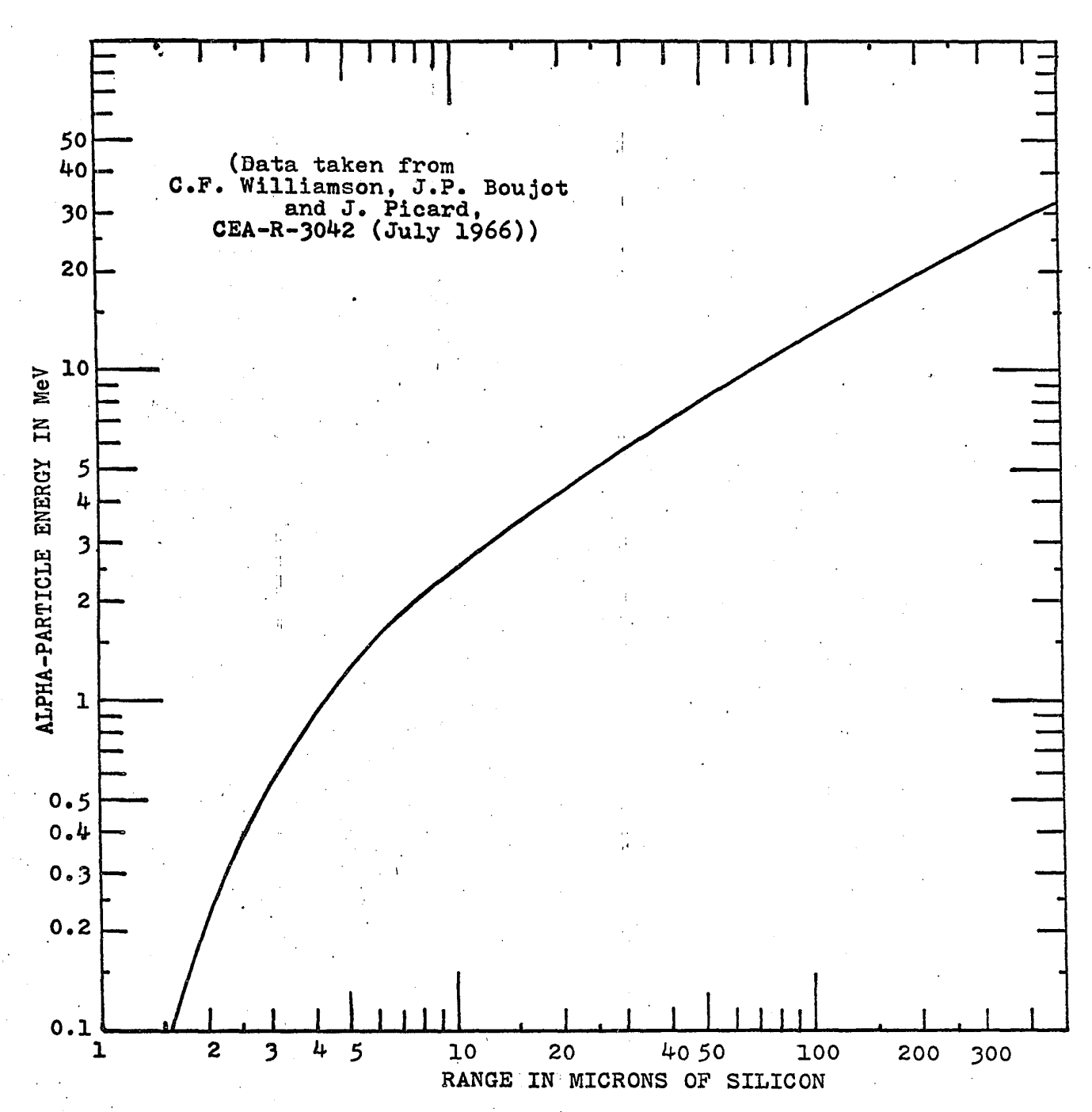


Fig. 4-9 Range-Energy Curve for Alpha-Particles in Silicon

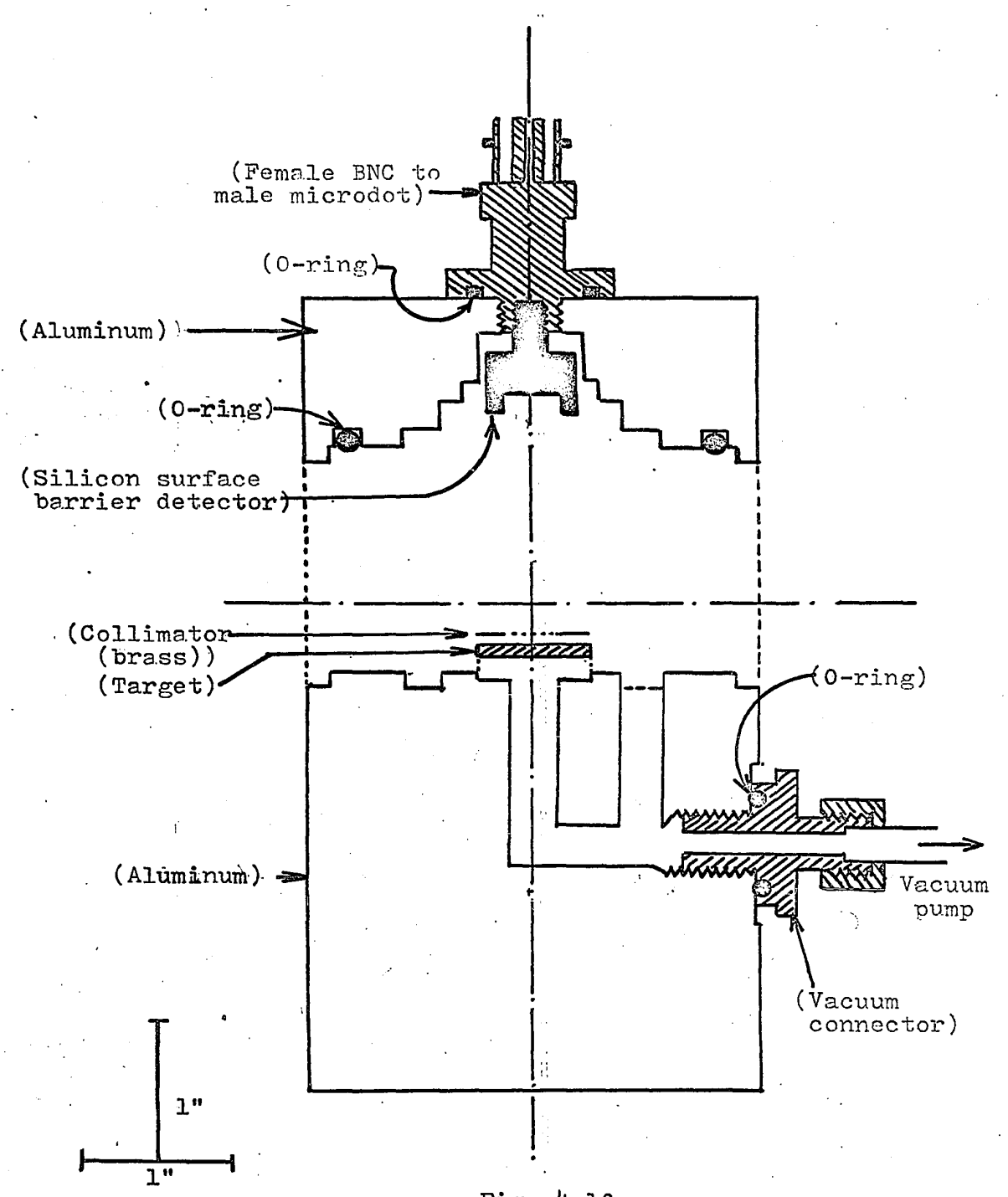


Fig. 4-10 Mechanical diagram of the detector chamber

the detector, viewed by the radioactive source. This collimator was used only for measuring the decay rates of the natural alpha-active target. The arrangement of the collimator with the non-bombarded target sources is included in Fig. 4-10.

A thin <sup>241</sup>Am standard source was used to check the system performance. The FWHM energy resolution with this source was better than 31 KeV on the 5.48 MeV alpha line. Typical resolutions obtained with the thorium targets used were of the order of 60 KeV FWHM for alpha-energies of about 8 MeV. Using this source the amplifier gains were set so that the energy range recorded and displayed by the analyser was 0 to 10 MeV. As mentioned previously, all count rates observed during the experiment were low enough to make system dead-time losses insignificant.

#### CHAPTER V

## PERFORMANCE AND RESULTS

#### V-l Introduction

If the first, second, third, etc., daughter nuclei produced in a radioactive decay are themselves radioactive and if their half-lives are much shorter than that of the parent, the number of atoms of each of the daughter products present is proportional to the products's half-life. This situation is described by the term "secular equilibrium". Such radioactive decay series exist for the heavy elements uranium, thorium, and neptunium; the stable end products of the series of the series are lead and bismuth isotopes. Secular equilibrium can also be attained when a radioactive substance is produced at a steady rate by some artifical method, such as a nuclear reaction in a cyclotron or chain-reacting pile. The condition for secular equilibrium occurs in the case of the parent isotopes 227Pa and 226Pa in this experiment, produced by the 232Th(p,6n)<sup>227</sup>Pa and <sup>232</sup>Th(p,7n)<sup>226</sup>Pa reactions respectively.

The members of decay chains which start from 227Pa and 226Pa have already been observed and are described in Table 5-1. The interrelation of the each of the series can probably best be seen by reference to a nuclide chart of the heavy region such as that shown in Fig. 5-0.

In this experiment, the threshold energies of 35.50 MeV for the  $^{232}$ Th(p,6n) $^{227}$ Pa reaction and 39.77 MeV for the

Table 5-1 (A) Collateral series data of 227Pa

Nuclide	Type of radiation	:	Energy of main alpha- radiation(MeV)	Percent of alpha-decay
227 <sub>Pa</sub>	α(~85%)* K(~15%)*	38.3±0.3 min*		50.7 11.8 15.2 9.6 2.6 8.0
223 <sub>Ac</sub>	α(99%)* K(1%)*	2.2±0.1 min*	6.659** 6.648 6.56 6.52 6.47	37.6 42.1 13.3 3.8 3.8
219 <sub>Fr</sub>	α(100%)*	0.02±0.002 sec*	7.30	98.4***
215 <sub>At</sub>	α(100%)*	10 <sup>-4</sup> sec, ±20%*	8.00****	100****
2ll <sub>Bi(A</sub>	cC) α(99.7%)	* 2.16 min*	6.619* 6.28****	84 <b>)</b> ;****
207 <sub>Tl(A</sub>	cC") в-#	4.76 min *	(Energy of \$ is 1.47 MeV)	
207 <sub>Pb</sub>	Stable	•		

data taken from:

<sup>\* =</sup> W. W. Meinke, A. Ghiorso, and G. T. Seaborg, Phys. ReV., 81 (1951) 782

<sup>\*\* =</sup> M. W. Hill, (1958), UCRL-8423, (unpublished)

<sup>\*\*\* =</sup> V. B. Subrahmanyam, (1963), UCRL-11082, (unpublished)

<sup>\*\*\*\* =</sup> G. Graeffe, P. Kauranen, J. Inorg. Nucl. Chem., 28 (1966) 933

<sup>\*\*\*\* =</sup> C. M. Lederer, J. M. Hollander, and I. Perlman,
"Table of Isotopes" sixth edition (1967),
John Wiley and Sons, Inc., New York

Table 5-1 (B) Collateral series data of 226Pa

Nuclide	Type of radiation	Half-life	Energy of main alpha-radiation(MeV)	Percent of alpha-decay (%)
226 <sub>Pa</sub>	α(74%) K(26%)	1.8±0.2 min**	6.863 6.823 6.728	52 46 1
222 <sub>Ac</sub>	α(≤98%) K(≥2%)	4.2 sec****	7.003 <b>)</b> * 6.957	93 <b>}</b> *
218 <sub>Fr</sub>	α(1,00%)·	pred. 5x10-3 <sub>se</sub>	2** 7.85 7.555 7.525	93 5 1
214 <sub>At</sub>	α(100%)* p	red. 2x10 <sup>-6</sup> sec		99*
210 <sub>Bi(RaE</sub>	) α(1.3×10 <sup>-4</sup> β (99+%)**	%)***** 5.0 da ***	ys** 4.69 **** 7.69 (Energy of mai radiation is	in beta-
210 <sub>Po(RaF</sub>	) α(100%)*	238 days**	5 • 3 • 305*****	100*****
206 <sub>Pb</sub>	Stable**			

## data taken from:

- \* = J. D. McCoy, Soc. Sci. Fennica, Commentations Phys.Math., 30, No.4 (1964), "Alpha decay studies of Pa-230, Pa-228, Pa-226 and their descendants".
- \*\* = W. W. Meinke, A. Chiorso, and G. T. Seaborg, Phys. Rev., 81 (1951) 782
- \*\*\* = " Nuclear Data" section B. vol.1, No.5, Nov. 1966 (editor: Katharine Way), Academic Press, New York
- \*\*\*\* = P. A. Tove, Arkiv Fysik, 13 (1958) 549
- \*\*\*\*\* = P. Kauranen, Ann. Acad. Sci. Femmicae, Ser. A, VI, 96 (1962) 1; Nucl. Sci. Abstr. 17, No. 2250 (1963)
- \*\*\*\*\* = C. M. Lederer, J. M. Hollander, and I. Perlman,
  "Table of Isotopes" sixth edition (1967)
  John Wiley and Sons, Inc., New York

Fig. 5-0

Nuclide chart for a portion of the heavy region

(Data taken from "Chart of the nuclides" by U. S. Atomic Energy Commission, Division of Isotopes Development.(1970))

\$\frac{1}{2}\frac{1}\frac{1}{2}\frac{1}{2}\frac{1}{2}\frac{1}{2}\frac{1}{2}\frac{1}{2}\frac{1}{2}\frac{1}{2}\frac{1}{2}\frac{1}{2}\frac{1}{2}\frac{1}{2}\frac{1}{2}\frac{1}{2}\frac{1}{2}\frac{1}{2}\frac{1}{2}\frac{1}\frac{1}{2}\frac{1}{2}\frac{1}{2}\frac{1}{2}\frac{1}{2}\frac		٠							. 4			· · · · · · · · · · · · · · · · · · ·											٠.		
Total   The   Th																	•			,					
Total   The   Th		•											N												
Total   The   Th		•									:		4	No 227	110229	No230	No 231	No 232	No 233	No234	71.755	No.236	Np2379	•No 238	4
Post   Tribute													Np	or 228	40m a 689	4 6m 4 666	l .	7 13m	2554	- G43-160	e e	>5.07 224 7.045	2:4:106/	212d 3 74 2	
Post											;	·		7 U227	U228		U230	U23I	11535	U2339	1/25	10235	1 237742		-1
The control of the co		• .				*						σ <sub>6</sub> 7.6	İ	1.1 m a 6 8 7	9.1 m a 669.652, y 25,.19,.15	0 6 36,6 33,6 30	0589,582,·· y072,154,25,	CIBI- 22		159 x 05y 74 32 479 - 73 42 39 5279	10:10:2		242 x 10'y		N. C. C. C.
The column   The						•					D <sub>0</sub>	Pa224		Pa 226	P0227 <sup>(5/-</sup>	229 0335	250.0333	E 37	J. 232	Pa 232	I Pa 233	2,95 0, 721 Da 222	Fg235	Po <u>236</u>	i
The content of the											1 '	0,6s a	~ 1s a 7 2 5	0 6.86,6.82,-		7.038-189 6.08,371-6.14 7.13-35	7.0424 0558.567.	- 055-165	7 513 34 7, 80, 9, 51	7,0475,047,771 0,760,975	12.C 2-4.F	1177- 630	31.4 <sup>4</sup>	e-13"	4
2009   1900   19	ТЬ	Th2I3	Th2I4	Th215	Th216	Th217	<u> </u>		Th220	Th221	Th222	Th223	Th224	726,028 Th2253	1 Th226	Th2272	728	l Th229ツ	Th270	Th 22 1:54	11.020	Th233	1577 24 63	<3m	
Column   C	232.038	.15s	.13s	1.25	28ms	<.5ms					~ 2.8ms a 7.98	a 7.3	y.177,···	y 322,362,246	y.II1,.242,131,··	y.25°, C/6·445	1 3 17	7.017-27 7,35	0466, 462 7568, 11-25 0, ~60, 51 ***********************************	709420,.017 .269	14.01.335 7.04.01.335 7.05	9-124.1 7-029-90 131450 0715	p 2674, (-5)	i	
12 CO FO	Ac2II	Ac212	Ac213			Ac216	ļ	Ac218	Ac2l9		Ac 221	Ac222	Ac223	Ac224	Ac225(3/-	Ac226	- <del>227</del> 97 	Ac228 3*	Ac229	Ac230	Ac 231	£1745	12.3		Ħ
\$\text{\$\text{\$\text{\$NOTE}\$}\text{\$\te	a 7.46			a 721,708,		2 9 11 2 9.03, 9.07 820,828		921	a 8.66 .	a 8.00,··	1	l <sup>e</sup>	e	6.139,**	1	7.06826 05.44?		078-164	ĺ	l				سنوز	1
1. 1. 1. 1. 1. 1. 1. 1. 1. 1. 1. 1. 1. 1	Ra 210		Ra2l2	Ra 213	Ra214	Ra215	Ra2l6			Ra 219	Ro220	Ro221	Ra222	Ro2239	1 Ra224	Ra22515/-	[5(72/26] [1602y	Ro227	Ro2		≤Ih			pisker.	
F 200 F 210 F 211 F 222 F 225 F 224 F 225 F 226	a702	a 6 91	g 6 87	a 662,673,	a 7.54	a 9 70,7.88,8.17	a 9.3	a 900			2746.690 y.465	6.665, 7.089,152,176, 221,0139		y 270, 031-580 g 130, g 1 2230185	224.0202	€ 39	7.185, 200 610	7 29, 50,027 El 31	7,~35				منتمنس .		
1.50	Fr 209	Fr 210	Fr 211	Fr 212	Fr 213	Fr2I4	Fr215	Fr216 Short	Fr 217	Fr 218 ~ 5ms	Fr 219	Fr 220	4.8m	Fr 222	۱ Fr223*	Fr 224	Fr225	Fr226		i .			-		
10 COS   Francis	a 6.65	a 6 57		6 54.	£2.10	848- 836,-	i		ļ.		219 0093	220 0123	y.218, 063*.45 no.6* 221.0142	E2 03	223.0197	€~31		D 00"	200						:
10	Rn 208	Rn 209	Rn 210	Rn 211'	Rn 212 25m	Rn2i3	Rn214	~ lµs	.05ms	.5ms	35ms	Rn 219 268176551,	Rn 220 55.6s 66 259.5747	Rn 221	RMS 38240	Rn 223	Rn 224 1.9h a-	KN225 4.5m g-	6m 6m						
Table 1	€ a 615 £~30	E~4.0	209 <u>98</u> 95	7 032-185 2578,585,562 7 069, 17, 23 E2 69	211 9907	2/2,9939	214.00	214.999	216.0003	217.0039		y.271,.401, 2130095	7542 7y < .2 220.0114	0 E~10	7.51 07~.72 222.0175					Ļ					
7	10	At 208 62h   1.6h	At209 <sup>3</sup>	8.3h		At 212 0125   0.225 0782, 0.766,	At 213 Short	~ 2µs	,IOms a 8,00,7.60	] .35ms	32ms	~ 25	0.9m	1			. •							•	
Copy	à 5.76 E 3.7	13565 E~50	5 3 40	23.35-5 32 E3.64	12448.y1.06,89. 13.65 17.0	2119937	212.993	213 9963	214 9987		noβ* 217,0046	β- 218.0086	219.0113	<u> </u>		1.1.2									
13 205° B) 206° B) 206° B) 20°	Po 206	1,62,33, 0.73		103y	P0 210	25a 77517 2736361607 1063 0.553	45s 11:03 a117: 0304µs	4µs	g 7.688,6.89	AGAN 1.78ms	<b>可YAN</b> 0.15s	<10s	a 6000,5.179				111								
1	a 5 22 E1 80	Ofm (23		91 208 392	7 209 98258 Di 2009	205556 BT.	72615 a 8 785 21196587	212.9928 Bi 212 !-	213 99520		Bi215	217.01		+											
PD   PD   PD   PD   PD   PD   PD   PD	15.3ld (5.8° 97 (7.703.1766.09	4377 C. 11 35	Place And Toronto	11,951 1O3A	100 y >2 x 10 y c (((mb + 19 mb)	310 y 27	266 214m 26622,6278,	770 60.60m - 727 765 - 160 (48 79 - 10 551	46m 8-142,102 y.440,	603 1764, 273 304 10.8m	7,4m (9/-) 8-							• '							
201 12 Admit 13 Admit	2.57 (02/2, 999 E 2 70	100 % rPh205	Ph 206	E297		Pb209	9 60 210 9973	Ph 21194	Pb 212	Pb 213	Pb 214			Ť											
TI 203"   TI 25"   TI 205"   TI 206   TI 207   TI 208"   TI 209"   TI 209	669m 1.48	44ms  3x107y	0126ms 23.6 (156.25b,30 963.88	0.80 22.6 11106 170 g.71	52.3 σ,∼i5πb	3.31h 8-64	2,	AGE 36.lm 3*137,55.** y405,632,427	10.64h 8*.34,58, 7.239,300,115	a-	8 69,74,103, 352,295,053		ļ									٠.	: "		
1g 200	TI 203*	ना 2	TI 2051	7 205,97590				°रा 210	E 58	I ~ 1.8	[E 104	-		<b>.</b>		-		<del>.</del>	•				· · · · · .		
1g 200	29.50 e/1.0	52μ•	70.50 σ <sub>y</sub> .7	# 4.2lm # 152 ************************************	144 , 90 141,31	97160,64-238 97160,64-238 9265,583,511,	2.2m p=18 , 120, 45,156	y 79, 30, 01 - 2 43				-													•
As (33.5%)	Hg 202	* Hg2O3*	Hg 204		Hg 206		E393	E547 •	<b>†</b>																
Au 201   Au 202   Au 203   Au 204   55s   55s   6743   55s   6743   55s   6743   65s	σ <sub>p</sub> 1.8	r 53, 94 10 212	9,1	y 205	<b>3</b> 9°																		•		
1200 Pt 201	Au 201	Au 202	Au 203	Au204	<b></b>	<b>†</b>									* -										
1 200 Pt 201   12h   2.5m   121   12t   15t	#"(5, y.53	8-35,	8-19	7 43																					
100 P	PI 200	Pt 201				1					٠.								•						
7 (76)	β (2 2, · ) γ(.568 · ( 62)) Β ( ~ 7	7176				j						•			*		7. <b>.</b> .								

.

232Th(p,7n)<sup>226</sup>Pa reaction are obtained from a set of nuclear-mass relations and a resultant mass table given by Garvey et al (47).

Preliminary bombardments of thorium targets in both the internal and external beam with energies ranging from 45 to 65 MeV established that the distinctive alpha-rays of the decay chains of protactinium-227 and -226 could be observed, and gave agreement with the half-lives and the percent of alphadecays of the Table.

## V-2 Performance and Data Reduction

To find any serious flaws in the design of the overall instrumental systems, each component was immediately tested after completely setting up the irradiation and counting system for runs.

Actual bombardments in the external beam were done for two and seventeen minutes in the  $^{232}\text{Th}(p,7n)$  and  $^{232}\text{Th}(p,6n)$  cases respectively. The irradiation periods depend on the activities under observation, which have half-lives of about 2 minutes for the (p,7n) reaction and 38 minutes for the (p,6n).

For accurate measurements of the mean energy of the degraded proton beam, the aluminum absorbers in the beam analyser box were the same as those described by Chang(4). The aluminum absorbers were cylindrical blocks with faces machined parallel to within 0.0025 mm. Individual blocks were weighed to an accuracy of 0.05%. The blocks were made of 99.8% pure

aluminum, the impurities being mostly elements for which the stopping power is very similiar to that of aluminum. Using a proton range-energy table given by Williamson et al (45), the overall accuracy of the proton range-energy relationship on aluminum is estimated to contain an error of less than ±0.2 MeV for the energy, as measured by Chang (4). The reproducibility of the range transmission graph ensures that the accuracy of the determinations of the mean energy and energy spread has a deviation of less than ±5 mg/cm², corresponding to an energy error of less than ±0.05 MeV. Consequently it is estimated that the absolute error of the measurements of both the mean external energy and spread are less than ±0.25 MeV. This result seemed to be slightly better than that of previous work by Turcotte (3) and Chang (4).

Immediately after the bombardments, the alpha-radiation was detected by the system previously described, having a total mean resolution of less than 47 KeV FWHM. The time intervals between the end of irradiation and the start of actual counting were 1.5 minutes for the  $^{232}(p,7n)$  reaction and a maximum of 5 minutes for the  $^{232}Th(p,6n)$  reaction. The energies of the alpha-radiations produced were identified using the energies of the natural radioactive thorium decay chain given in Appendix II, and those of a mixed standard alpha-source consisting of 5.15 MeV in  $^{239}Pu$ , 5.48 MeV in  $^{241}Am$  and  $^{244}Cm$ . It was decided to choose the 8.00 MeV peak of the

daughter 215At, produced in the 227Pa decay chain following the 232Th(p,6n) reaction, and the 7.85 MeV peak of the daughter 218Fr from the 226Pa decay chain following the 232Th(p,7n) reaction. These peaks stand out clearly in spectra, and have strong relative intensities.

In equation (3-14), which was used in the cross-section calculations, the only quantities not directly measured in this experiment were the decay constants  $\lambda$  and  $\lambda_n$ , and the branching ratios Z and Z'. These are given in Table 5-1, and an example of a calculation is given in Appendix II.

In the data reduction, two kinds of errors occur, systematic or constant errors, and random errors. The constant errors are associated with the absolute branching ratios of Z' and Z, the disintegration constants  $\lambda$  and  $\lambda_n$ , and the area S. The systematic errors are associated with the time intervals. The random errors are associated with the number of protons P, the dead time corrections of Y and Y', the number of recorded counts  $R_a$  of induced radioactivity, and the natural decay rate  $Q=(dN_n/dt)_cS$ .

No attempt was made to evaluate the constant error in  $\lambda$ ,  $\lambda_n$ , Z, Z' and S. Also the systematic errors due to measurements of t,  $t_1$ , and  $t_2$  were not evaluated, since these are insignificant. According to the pulse widths, and observed count rates, there is essentially no dead time correction necessary. The random errors of  $Q=(dN_n/dt)_cS$  and  $R_a$  are significant, however; the error in the natural decay rate  $Q=(dN_n/dt)_cS$  was of the order of  $\pm 2\%$ .

Most statistical errors due to the number of recorded counts  $R_a$  of induced activity were given by about  $\pm 2.5\%$  for the  $^{232}\text{Th}(\text{p,6n})$  reaction and about  $\pm 10\%$  or less for the  $^{232}\text{Th}(\text{p,7n})$  reaction. As discussed by Kavanagh et al (2), the errors of measurement in the number of protons P is due to the efficiency of the standard Faraday cup in the collection of proton charge, and the errors arising from forward and backscattering of the incident protons from the target; these were checked to be insignificant by testing beam transmission into the cup with and without the target in place. The resultant error of measurement of P is estimated to be better than  $\pm 2\%$  on the average.

Using the law of propagation of errors, the resultant total random errors for the cross-section measurements in most cases are given by about  $\pm 4\%$  for the  $^{232}\text{Th}(p,6n)$  reaction and about  $\pm 12\%$  for the  $^{232}\text{Th}(p,7n)$  reaction.

# V-3 Results and Discussion

## A. Experimental Results

The cross-sections for the  $^{232}{\rm Th}(p,6n)^{227}{\rm Pa}$  and  $^{232}{\rm Th}(p,7n)^{226}{\rm Pa}$  reactions measured at various proton energies up to 102.00 MeV are presented in Tables 5-2 and 5-3 respectively, and the excitation functions are plotted in Fig. 5-1. These excitation functions are similar in form to the many (p,xn) cross-sections described in previous work (1,3,4,6,7,8,10).

The excitation function presented in Fig. 5-1 for the

Table 5-2 Experimental  $^{232}$ Th(p,6n)  $^{227}$ Pa cross-sections

Incident proton energy (MeV)	Energy spread of proton beam(FWHM) (MeV)	Cross-sections (mb)				
38.80	1.00	3.02 ± 0.48				
40.54	1.30	9.28 ± 0.55				
42.72	. 1.30	24.66 ± 1.46				
45.28	1.11	$38.70 \pm 1.44$				
47.44	1.28	41.57 ± 1.41				
48.90	1.28	39.69 ± 1.40				
49.52	1.25	35.79 ± 2.05				
50.48	1.20	30.33 ± 1.04				
51.70	1.20	$26.07 \pm 0.72$				
53.60	1.41	22.82 ± 1.56				
56.15	1.30	14.96 ± 0.57				
62	1.0%	10.24 ± 0.42				
70.	1.0%	$8.01 \pm 0.34$				
80.00	1.0%	7.18 ± 0.27				
90	1.0%	5.87 ± 0.25				
102.0	1.0%	4.95 ± 0.27				

<sup>\*</sup> estimated spread of proton beam (FWHM)

Table 5-3
Experimental <sup>232</sup>Th(p,7n)<sup>226</sup>Pa cross-sections

Incident proton energy (MeV)	Energy spread of proton beam (FWHM) (MeV)	Cross-sections (mb)
50.39	1.28	2.30 ± 0.73
51.68	1.25	$3.29 \pm 0.88$
52.91	1.29	5.97 ± 1.03
<i>55</i> <b>.</b> 88	1.25	12.06 ± 1.30
56.66 .	1.12	12.24 ± 1.42
59.19	1.38	11.65 ± 1.40
59.78	1.20	10.68 ± 1.12
62.51	1.19	$7.40 \pm 0.86$
64.90	1.00	6.74 ± 0.76
66.70	1.27	5.77 ± 0.91
69.26	1.12	4.56 ± 0.61
71.13	1.12	3.31 ± 0.48
74.40	1.01	$3.29 \pm 0.53$
78.80	1.02	2.96 ± 0.50
88.78	0.90	$2.60 \pm 0.35$
102.00	1.00	2.34 ± 0.38

# Fig. 5-1

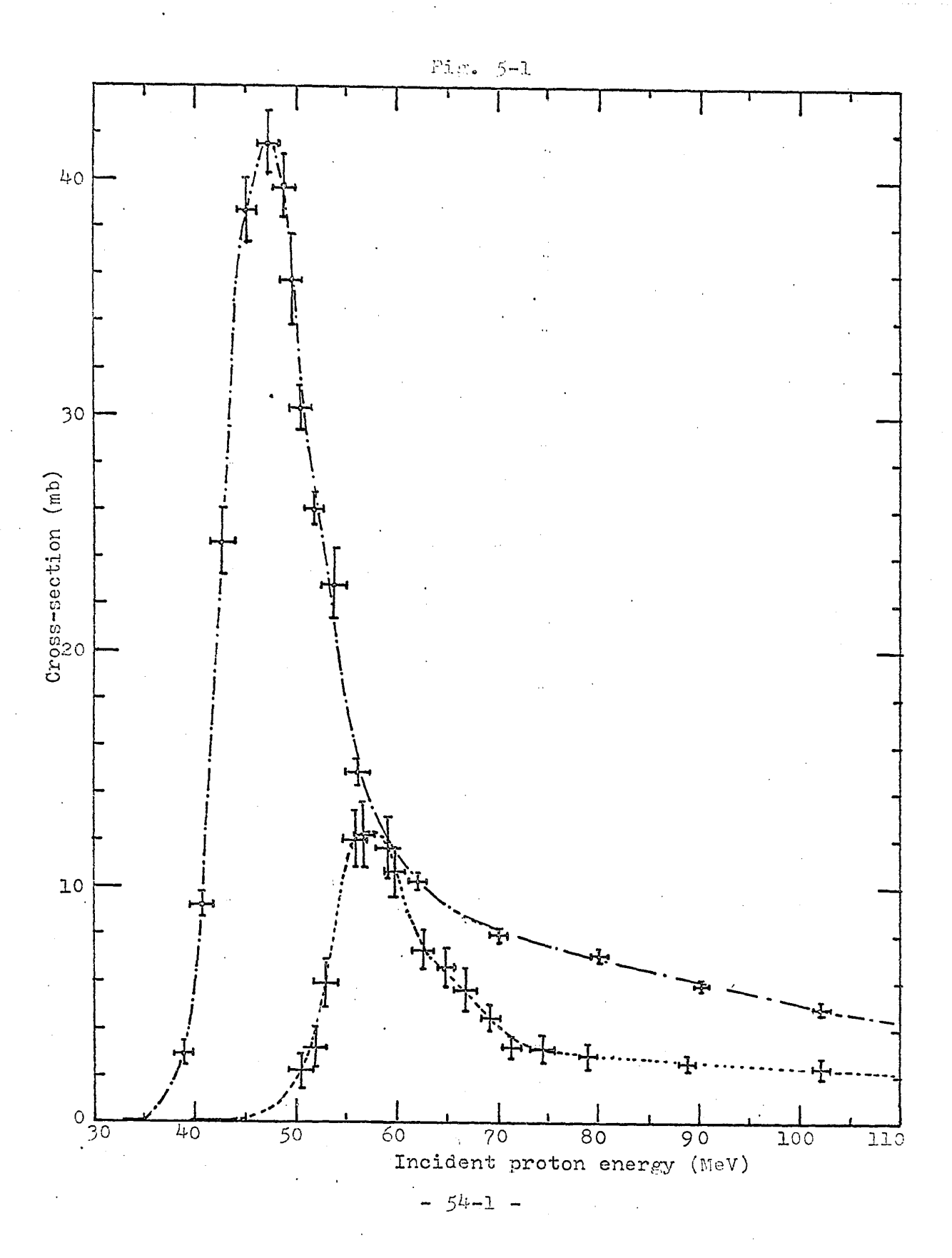
The measured excitation functions for the  $^{232}$ Th(p,6n) and  $^{232}$ Th(p,7n) reactions. (The dashed and dotted curves are intended only to guide the eye, and are not comparisons with theory.)

-:232 $_{\text{Th}(p,6n)}$  excitation function +:232 $_{\text{Th}(p,7n)}$  excitation function

( Horizontal error bars represent the spread in beam energy.

Vertical error bars are from background subtraction

and counting statistics.)



(p,6n) reaction shows a suprisingly sharp peak. The cross-section for the production of 227Pa from 232Th has a threshold of 32.50 MeV and rises sharply to a maximum value of 43 mb at 47 MeV. On the high energy side of the peak, above about 60 MeV, the curve becomes asymmetric with a tail extending up to the maximum bombarding energy. A slight anomaly appears at about 55 MeV, possibly due to a different reaction mode. The excitation function presented in Fig. 5-1 for the 232(p,7n) reaction is similiar in form the 232Th(p,6n) case, rises from a threshold of 37.77 MeV to a maximum value of 13 mb at 57 MeV, (about 10 MeV higher than the 232Th(p,6n) peak). Again on the high energy side of the peak another reaction mode becomes apparent at about 65 MeV, superimposed on a long tail.

Presumably both tails correspond to events caused by the prompt emission of one or more neutrons followed by the delayed emission of the remaining ones.

#### B. Comparison with Other Experimental Results

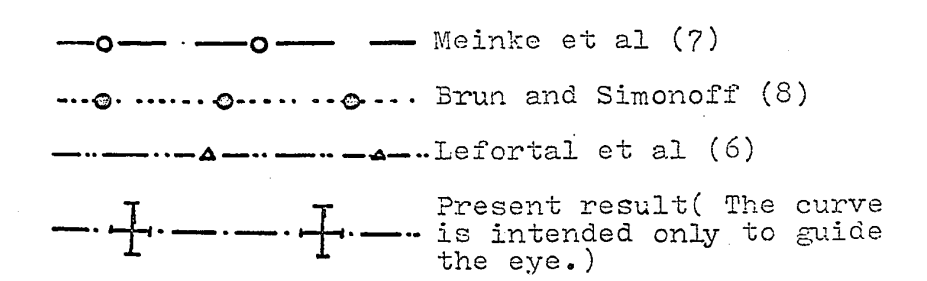
Using the electrostatically deflected proton beam of the 184-inch synchrocyclotron, Meinke et al (7) bombarded stacked foils of 5 mm thorium, with varying thicknesses of copper metal sandwiched between the sixteen foils in each case. After bombardment, the 0.4 gram of thorium were removed and dissolved in concentrated nitric acid. The proton energy measurement in this experiment was very crude because of the spread in the initial energy of the incident particles and the straggling in

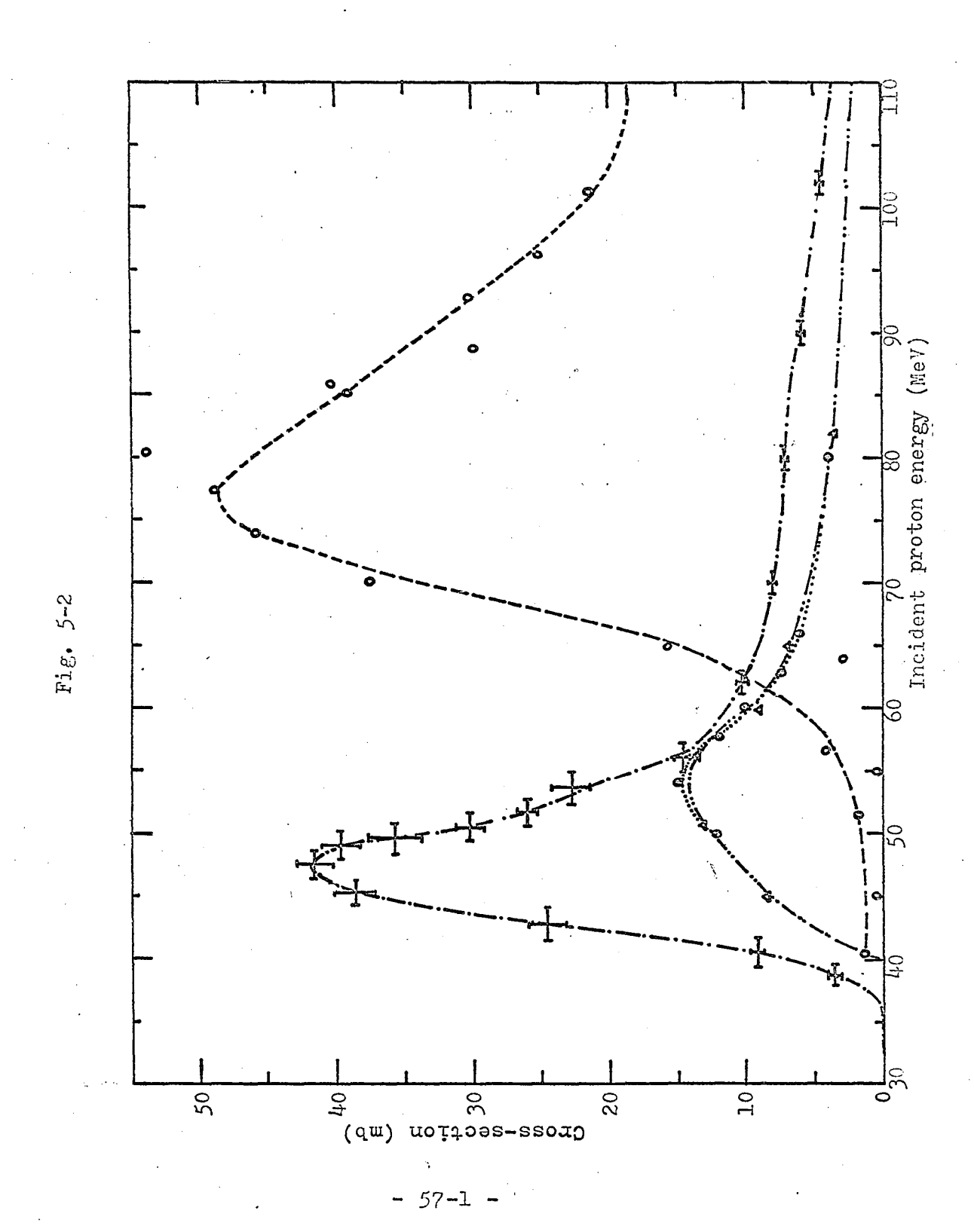
the stacked foils. Their experimental result for the 232Th(p,6n) reaction is included in Fig. 5-2 which shows only the low energy portion of their measurement. The excitation function rises to a maximum of 50 mb, which is slightly higher than the present result. The main discrepancy between Meinke's result and the present experiment is in the position of the peakat 80 MeV in Meinke's experiment, compared to 47 MeV in ours.

Lefort et al (6) and Brun and Simonoff (8) likewise obtained absolute cross-sections for proton energies up to 155 MeV, which are also included in Fig. 5-2. Both experiments were carried out using aluminum and carbon monitor foils, chemical separation of the targets after bombardment, and alphaparticle counting. The targets used in both experiments were in most cases thicker than those used in the present experiment (about 200-300 ug/cm<sup>2</sup>). The excitation functions in both cases appear to reach a maximum between 13 and 15 mb at about 54 MeV in disagreement with both the peak height and peak position of the present experiment. There are a number of possible sources of error involved in the previous measurements, all of which may account for the discrepancy with the present result. main difficulty is undoubtedly the large energy spread introduced in a beam degraded to about 50 MeV from a much higher incident energy; this is inevitable in the earlier experiments involving stacked foils. The earlier experiments also involved chemical separation techniques, which were not required in the present

Fig. 5-2

Comparison of  $^{232}\text{Th}(p,6n)^{227}\text{Pa}$  excitation function with previous experimental results:





work.

No attempt was made in the earlier experiments to find the  $^{232}\text{Th}(p,7n)$  cross-sections (probably because of the short life-time of  $^{226}\text{Pa}$ ). To our knowledge this is the first such measurement.

## C. Theoretical Considerations

Equation (2-5) expresses the cross-section predicted according to Jackson's theory (10). A comparison with the detailed Jackson model (10) is difficult unless the variation of residual excitation energy in the case of each of the prompt processes is known. The Jackson model (10) involves averaging the term  $P(E^*, x-i)$  over such a distribution. To be able to find  $P(E^*, x-i)$  we must know the probability that a collision with an incident energy  $E_0$  will leave the nucleus with an excitation energy  $E^*$ . If this is known,  $P(E^*, x-i)$  can be calculated. The cross-section could then be calculated from

$$\sigma_{\text{th}}(p,xn) = \sigma_{c}(E_{o}) \{ q(0,0)P(E^{*},x) + q(1,0) < P(E^{*},x-1) > + \ldots \} (5-1)$$

Jackson (10) suggests that a) above 60 MeV the theoretical probability for compound nucleus formation q(0,0) is smaller that the probability for the ejection of one prompt neutron q(1,0) and is of the same order as the probabilities for emission of two prompt neutrons q(2,0); b) the probability of a residual excitation energy E\* in the case of a prompt q(1,0) event at incident energies below 100 MeV is roughly proportional to E\*;

c) in the case of higher order prompt q(2,0) events, the distribution is rectangular.

To include contributions from the 2nd, 3rd terms, etc., in equation (5-1) requires a more detailed knowledge of the probability of residual excitation E\* with incident energy than is presently available, to make a meaningful comparison with theory. Therefore, in the present work we have attempted only to fit the data with the first term of the series in equation (5-1), i.e., as though the event involved only delayed evaporation of 6 neutrons for the 232Th(p,6n) reaction and 7 neutrons for 232Th(p,7n) reaction. In each of the delayed cases, one is not concerned with an averaging over residual excitation probability, since the excitation energy of the target has a definite value. Thus the theoretical cross-section formula can be written as

$$\sigma_{th}(p,xn) = \sigma_c(E_0) q(0,0) P(E^*,x)$$
 (5-2)

resulting in a combination of the Jackson (10) and Blatt and Weisskopf (11) model. In equation (5-1), the  $P(E^*,x)$  involves Pearson's incomplete gamma function, given in equation (2-7) which must be integrated by parts. Using equations (2-6) and (2-7),  $P(E^*,x)$  in equation (5-2) can then be written as

$$P(E^*,x) = e^{-\Delta_{X+1}} \int_{0}^{a_1} (\Delta_{x+1}^{a_1}/a_1^*) - e^{-\Delta_{X}} \int_{0}^{a_2} (\Delta_{x}^{a_2}/a_2^*) (5-3)^{\dagger}$$

<sup>†</sup> This formula is quoted by Lefort et al (6); however there is a mistake in the signs of the terms in their paper.

where  $a_1 = 2x-1$  and  $a_2 = 2x-3$ . Therefore, equation (5-2) becomes

$$\begin{split} \sigma_{\rm th}(p,xn) &= \sigma_{\rm c}(E_{\rm o}) \; q(0.0) \big\{ e^{-\Delta_{\rm X+l}} \sum_{0}^{a_{\rm l}} (\Delta_{\rm X+l}^{a_{\rm l}}/a_{\rm l}!) \\ &- e^{-\Delta_{\rm X}} \; \sum_{0}^{a_{\rm 2}} (\Delta_{\rm X}^{a_{\rm 2}}/a_{\rm 2}!) \big\} \end{split} \tag{5-4}$$

In order to find the variation of the theoretical cross-section with the nuclear temperature, i) the reaction cross-section  $\sigma_{c}(E_{o})$ , for an incident proton of energy  $E_{o}$  was taken from Shapiro (14), and was calculated for values of  $E_{o}$ up to 100 MeV. In this calculation the nuclear radius parameter  $r_0$  used in the formula  $R = r_0 A^{1/3}$  was taken to 1.30 fm; ii) the relative probability q(0,0) for the emission of no prompt neutrons and no protons was taken from Jackson (10); iii) a program was written for the PDP-15 computer to calculate the  $P(E^*,x)$  values for the  $^{232}Th(p,6n)$  with a threshold of 32.50 MeV and for the <sup>232</sup>Th(p,7n) with a threshold of 39.77 MeV. In order to find the best fit to the present experimental points, the P(E\*,x) values were computed for nuclear temperatures ranging from 1.0 to 1.8 MeV; these appear in the expression  $\Delta_{\rm v}$  =  $(E^* - \sum_{i=0}^{X} B_i)/T = (E_o - E_{th})/T$ , where  $E_{th}$  is the threshold energy of a given reaction.

The results of the theoretical analysis using equation (5-4) are presented in Fig. 5-3 in the form of excitation functions which are seen to vary with the nuclear temperature T.

The shape of the curves thus obtained is nearly identical to the shape of the  $P(E^*,x)$  curves themslves; in this range  $\sigma_C(E_0)$  is rising slowly, while q(0,0) is decreasing. At the peak the theoretical cross-section is very much higher than that measured experimentally. It is believed that the competition of fission events with nuclear evaporation is the most likely reason for this discrepancy. This will be discussed in more detail later.

It is seen that the curve for T=1.1 has its peak at the same energy (47 MeV) as the experimental curve of the (p,6n) excitation function. Fig. 5-4 shows the theoretical curve for T = 1.1 MeV normalized to the same peak height as that of the experimental data. It is seen that the agreement in the shape is excellent up to a proton energy of 52 MeV, above which the experimental points exhibit the expected higher energy tail. The position of the peak is quite sensitive to the choice of nuclear temperature T. A change of 0.1 MeV in nuclear temperature shifts the peak position by roughly 1 MeV.

Similiar calculations have been performed for the  $^{232}$ Th(p,7n) reaction. In this case the variation of theoretical cross-section with nuclear temperature is also represented in Fig. 5-3. The nuclear temperature which corresponds to the experimental peak cross-section is 1.3 MeV in the curve of best fit shown in Fig. 5-4. This curve which, as in the (p,6n) case overestimates the measured cross-section, has been

## Fig. 5-3

Variation of theoretical excitation function with nuclear temperature according to equation (5-4);

Theoretical 232Th(p,6n) cross-sections;

T = 1.0 MeV ----
T = 1.1 MeV ---
T = 1.2 MeV ---
Theoretical 232Th(p,7n) cross-sections;

T = 1.2 MeV ----
T = 1.3 MeV ------

T = 1.4 MeV -----

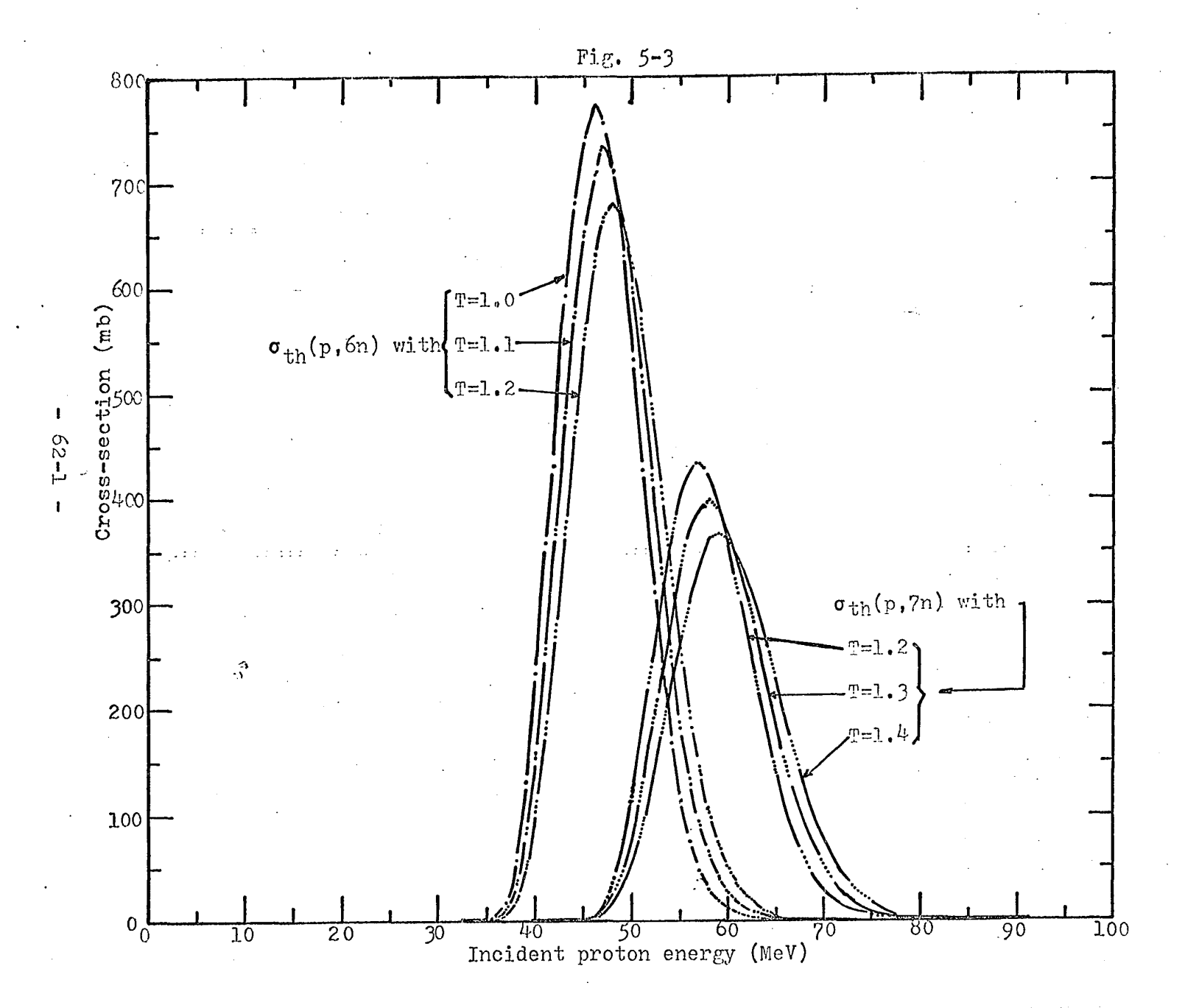


# Fig. 5-4

Theoretical  $^{232}{\rm Th}({\rm p.6n})$  cross-section normalized to the same peak height as the experimental points.

(Nuclear temperature T = 1.1 MeV, Normalization factor =  $5.7 \times 10^{-2}$ )

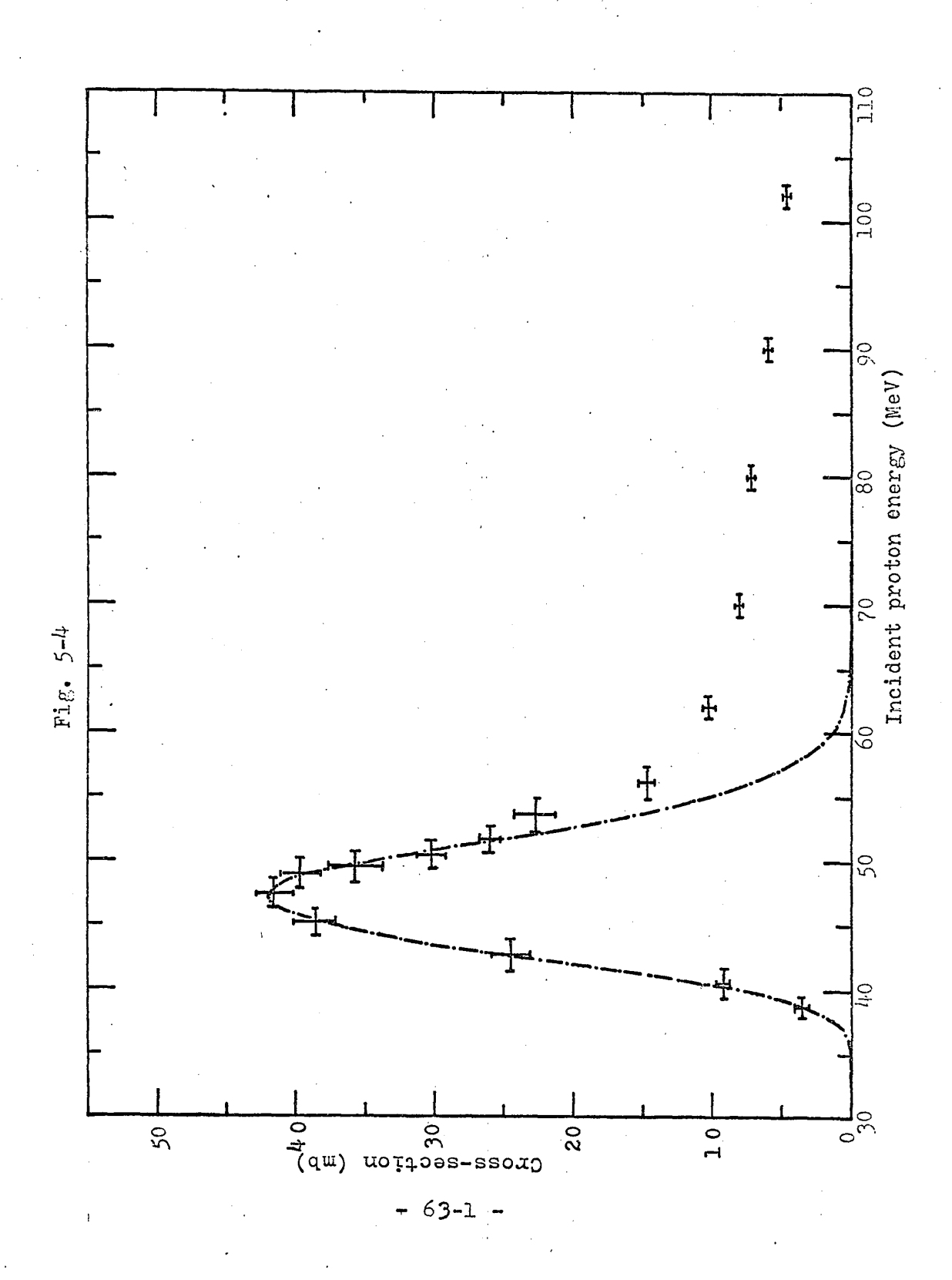
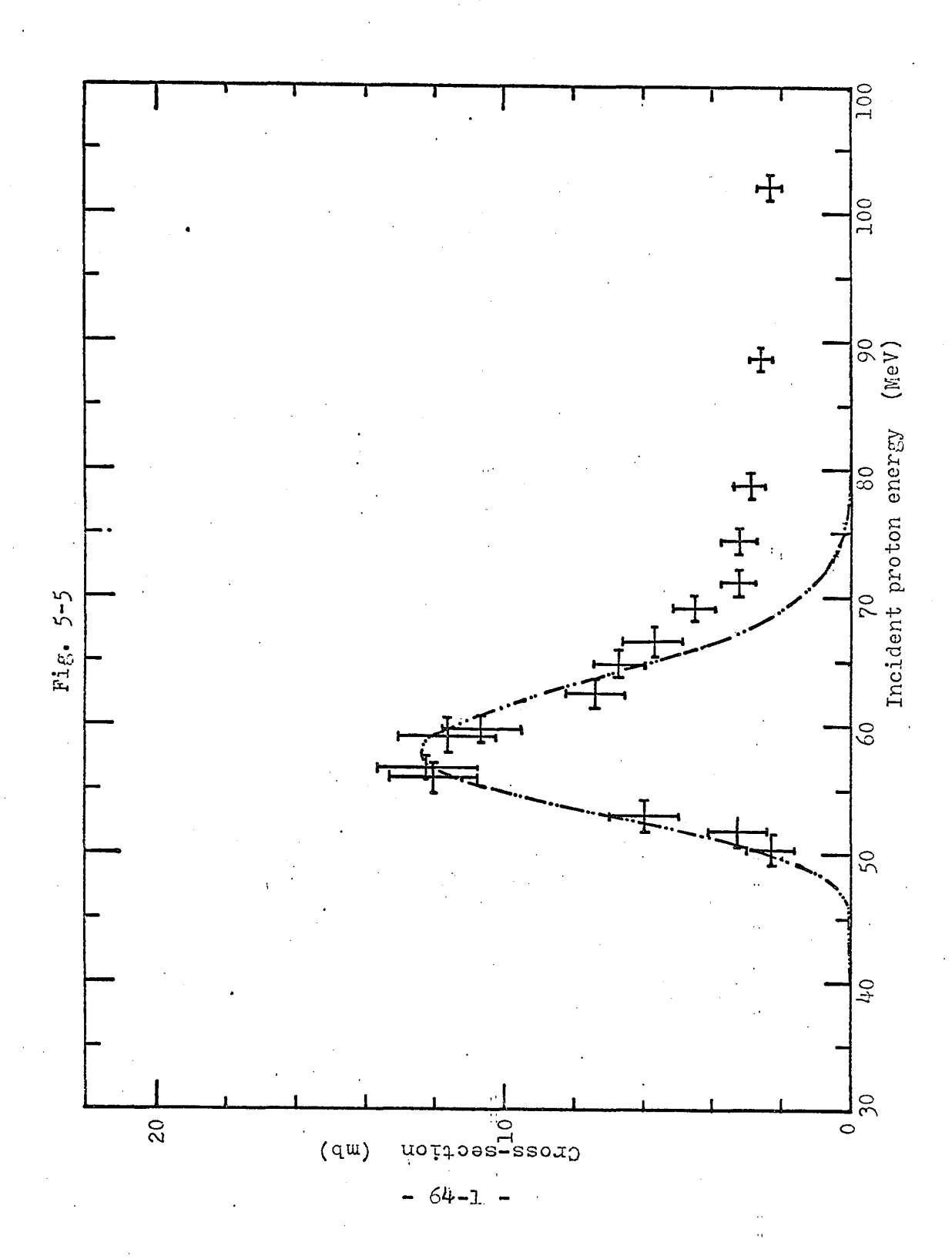


# Fig. 5-5

Theoretical  $^{232}$ Th(p,7n) cross-section normalized to the same peak height as the experimental points.

( Nuclear temperature T = 1.3 MeVNormalization factor =  $3.06 \times 10^{-2}$ )



normalized to the same peak hight as the experimental points. In this case, the shape agreement is excellent up to an energy of 65 MeV, above which the experimental points again show the expected high energy tail.

The values of T = 1.1 MeV for 232Th(p.6n), and 1.3 MeVfor 232Th(p,7n) are lower than those obtained in experiments carried out in previous (p.xn) reactions in this mass region, and are low compared to previous theoretical estimates. the work of Bell, Skarsgard and Jackson (1, 10) on 206pb, 207pb, and <sup>209</sup>Bi, the temperature used to fit the data was 1.8 MeV. Lefort et al (6) used a temperature T = 1.9 MeV to fit their results for <sup>232</sup>Th(p,6n). These values agreed resonably well with the theoretical estimates of Blatt and Weisskopf (11), which were based on the Fermi gas model of heavy nuclei; according to this model the nuclear temperatures T and excitation E\* should be represented by  $E^* = aT^2$  where a is a constant related to the nuclear level density. According to Blatt and Weisskopf (11), the value of a, for a nucleus with A=231 was quoted to be roughly 12 MeV-1. This figure was extracted from data available at that time from the known levels of odd-A nuclei in the neighbourhood of 1 MeV. With this estimate of a, the expected value of T for an excitation energy of about 50 MeV would be 2 MeV, which makes the values used by Lefort et al (6) and Jackson (10) quite plausible.

These values of T are not, however consistent with

estimates made by Turcotte (3) of nuclear temperatures in a number of (p,xn) studies done on the target  $^{127}I$ . Turcotte (3) fitted (p,3n), (p,6n), and (p,7n) data with a nuclear temperatures of 1.55 MeV, and (p,8n) with a temperature of 1.85 MeV. In one case (p,5n), the value T=1.20 MeV was used. Since, in Blatt and Weisskopf's derivation (11) the constant a is related to the level density W(E) by the relation

$$W(E) = C \exp(2\sqrt{a E^*})$$
 (5-5),

a lower nuclear temperature should imply a higher value of  $\underline{a}$ , which in turn suggests that in  $^{127}\text{I}$  the level density should be higher than in  $^{232}\text{Th}$  and  $^{208}\text{Bi}$ . This seems unreasonable. It would be more consistent to conclude that the earlier experiments led to unreasonably high T values; if this is true, the values of temperature quoted in the present experiment are consistent with those of Turcotte (3), for the lighter target nucleus  $^{127}\text{I}$ . (The possible sources of error in the earlier measurements have already been discussed.)

Many authors have discussed possible modifications of the Blatt and Weisskopf (ll) treatment. For example the nucleus may be considered to "cool off" during the evaporation process (48) so that the effective temperature is lower than the value estimated from  $T = (E*/\underline{a})^{\frac{1}{2}}$ . Brun and Simonoff (8) used a calculation based on work by Tarrago (49) in which the temperature is estimated not from the initial excitation,

but from a mean value calculated along the evaporation chain.

It is therefore not reasonable to consider the nuclear temperature as a reaction constant - nevertheless this parameter should provide a useful comparison of level densities in different nuclei, with comparable initial excitations.

Blatt and Weisskopf (11) mention that the values of C and a in equation (5-5) were adjusted to fit the level data then available, and should be considered only a rough guide to the general features of level densities. If their values C = 0.005 MeV<sup>-1</sup> and a = 12 MeV<sup>-1</sup> are used, equation (5-5) gives a level density of 5.5 MeV<sup>-1</sup> for A=231 in the neighbourhood of 1 MeV excitation. The isotope table of Lederer et al (50) shows 10 levels below 0.5 MeV in <sup>233</sup>Pa, and a glance at other odd A nuclei in this region shows level densities close to 20 MeV<sup>-1</sup>. This again suggests a value of a larger than Blatt and Weisskopf's (11) earlier estimate. It is, then, not unreasonable to conclude that such revisions in the earlier estimates of level densities, and more realistic evaporation calculations could yield values of T which are consistent with the measurement in the present experiment.

D. Competition of Neutron Evaporation with Fission

The discrepancy between the shape of the theoretical curves and the position of the experimental points is not surprising since the contribution of prompt neutron emission has been neglected. Although the shape of the q(1,0) and

q(2,0) curves (Fig. 1 in ref. 10) suggests that inclusion of these prompt evempts would add a high-energy tail to the theoretical curves, it should not appreciably add to their peak height. The very large discrepancy between the peak height of the experimental and theoretical excitation functions suggests that some competing process has been ignored; the fact that the theoretical curves can be normalized to fit the experimental ones suggests that the excitation function for the competing process has the same shape as that of neutron emission.

A number of earlier papers (6,8,51, 52, 53,54) have discussed the relative probabilities of neutron emission, and induced fission in the heavy elements. Based on many cross-section measurements for both fission inducing reactions, and others involving neutron cascades, data have been compiled on estimates of  $\lceil n/\lceil f \rceil$ , the ratio of the relative widths of neutron decay to fission. Lefort et al (6) present a partial list of  $(\lceil n/\lceil f \rceil)$  ratios suitable for atomic masses ranging from 226 to 238. Fig. 5-6 of their paper shows a plot of  $\log(\lceil n/\lceil f \rceil)$  vs. A for many data points. It is apparent that the data are well fitted by a set of essentially parallel straight lines, one for each Z value. An empirical relationship, then, which should represent  $(\lceil n/\lceil f \rceil)$  values, is therefore

$$(\lceil n/\rceil = C(Z) \exp(kA)$$
 (5-6)

An identical relationship was suggested in an earlier paper (53), and a value of k=0.335 was estimated from a fit to ll ratios available for the isotopes of uranium.

Fujimoto and Yamaguchi (51) have estimated the relative values of  $\Gamma_n$  and  $\Gamma_1$  in a theoretical derivation based on the Fermi-gas model of the nucleus. The fission width estimate is

$$\Gamma_{f}(E) \approx T/2\pi \exp(-E_{f}/T)$$
 (5-7)

where E is the excitation energy,  $E_{\mathrm{f}}$  is the fission threshold, and T (the nuclear temperature) is assumed to be proportional to the square root of the excitation energy. The neutron width, using the same model is

$$\Gamma_{\rm n}(E) \approx 1/2\pi \ ({\rm A}^{2/3}/{\rm K}^{\, \cdot}){\rm T}^2 \ \exp(-{\rm B}_{\rm n}/{\rm T})$$
 (5-8)

where  $K^r = \hbar^2/2mr_0 \approx 10$  MeV, and  $B_n$  is the neutron binding energy. The ratio of widths is therefore

$$\Gamma_{n}/\Gamma_{f} = TA^{2/3}/10 \exp\left[\left(E_{f}-E_{n}\right)/T\right] \tag{5-9}$$

For  $^{233}$ Pa,  $E_f = 4.59$  MeV and  $B_n = 6.70$  MeV.(54). Neglecting the abrupt jump in binding energy between neighbouring odd-odd and odd-even isotopes, the value of  $E_f$  increases at a rate of about 0.12 MeV per nucleon, while  $B_n$  decreases by about 0.13 MeV per nucleon. Equation (5-9) therefore predicts that the plot of  $\ln(\lceil n/\lceil \frac{\pi}{2} \rceil)$  vs. A should be linear, with a

slope of 0.25/T, which, for low nuclear temperatures, is in fairly good agreement with the slope of 0.335 of the data compiled by Lefort et al (6) and Lindner and Turkevich (53). It therefore seems reasonable to use equation (5-6) to compute values of  $\Gamma_n/\Gamma_f$  along the neutron decay chain. In the calculation which follows, the value of k is assumed to be 0.335, consistent with the earlier experiments, and C is selected to give reasonable agreement to the normalization constant of 5.7 x  $10^{-2}$  found in our experiment. The logarithmic form of equation (5-6) is

$$ln(\Gamma_n/\Gamma_f) = ln C + 0.335 A$$
 (5-10)

The value of lnC = 77.62 is found to be consistent with the normalization constant in the  $^{232}$ Th(p,6n) reaction. This calculation is shown in Table 5-4. The first column lists the values of A for Pa isotopes along the decay chain, and the second column gives the value of  $\Gamma_n/\Gamma_f$  for each value of A. In each step of the decay process the neutron width: total width ratios will be  $\Gamma_n/\Gamma_n+\Gamma_f$ ), which is shown in column 3. The cumulative product  $\Gamma_{i=1}^X$ , which represents the overall neutron width: total width, in the evaporation of x neutrons, is shown in column 4. The last column should represent the normalization constants required in  $^{232}$ Th(p,xn) measurements to account for fission competition. The figure of 0.020 for the (p,7n) case agrees reasonably well with the measured value

Table 5-4

A	([n/[²])	$\lceil n/(\lceil n+\rceil_f) \rceil$	$\prod_{i=1}^{x} \left( \frac{\Gamma_n}{\Gamma_n + \Gamma_n} \right)$
233	4.20	0.808	0.808
232	3.00	0.750	0.606
231	2.05	0.672	0.407
230	1.54	0.606	0.247
229	1.10	0.524	0.129
228	0.785	. 0° 14170	0.057
227	0.563	0.360	0.020

of  $3.06 \times 10^{-2}$ , considering the approximations involved in the theories of fission competition and neutron evaporation.

Fig. 5-6 shows the values of  $(\lceil n/ \rceil_1)$  which were compiled and plotted by Lindner and Turkevich (53). Added to this graph is the line corresponding to the value C = 77.62. This lies between the two previous estimates of the  $\lceil n/ \rceil_1$  ratios for Pa which were calculated on the basis of spallation yields from uranium and thorium targets. We conclude, then, that fission competition explains satisfactorily the values of the normalization constants derived in this experiment.

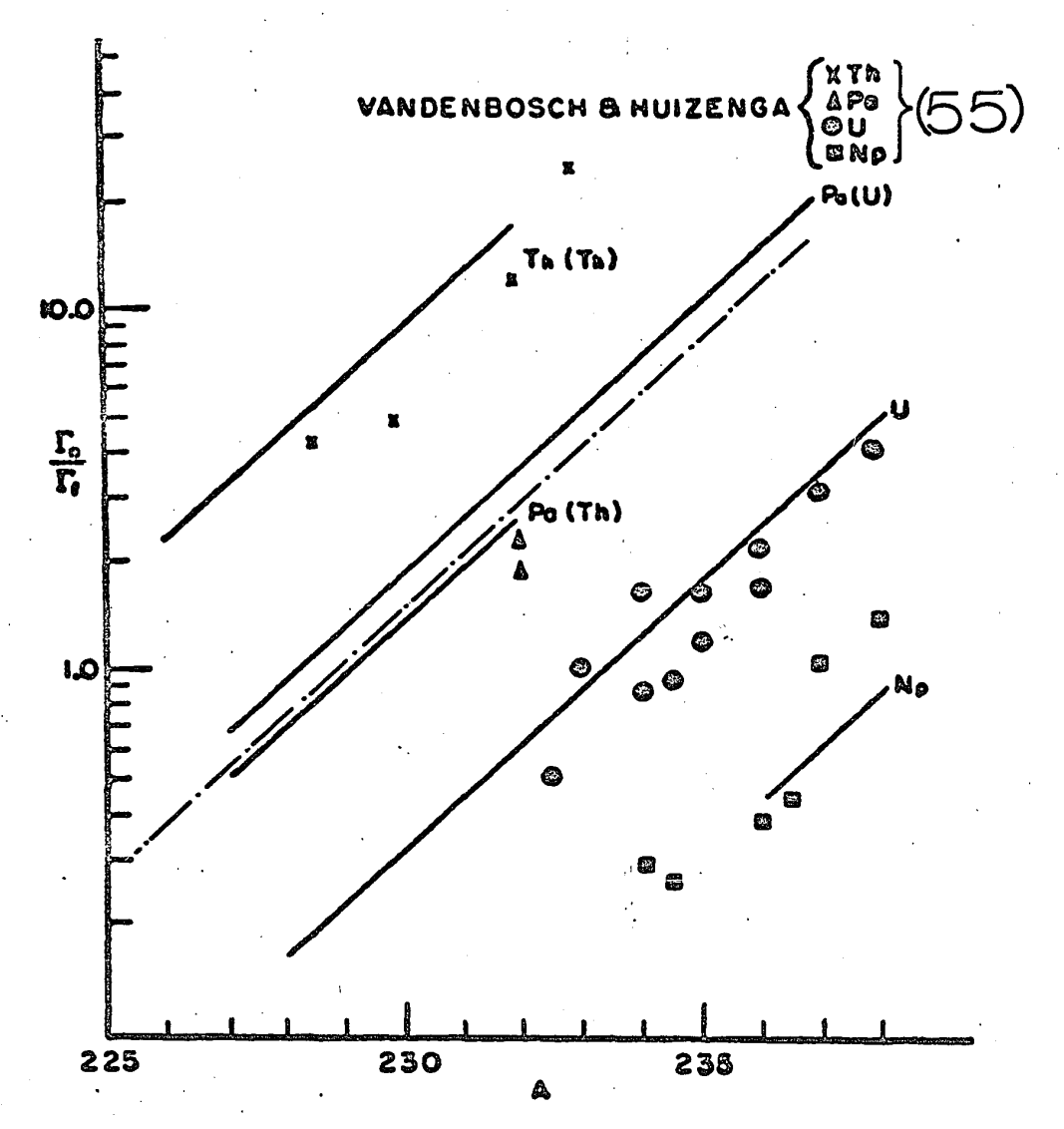
Fig. 5-6.

 $\Gamma_n/\Gamma_n$  as a function of A for fissionable nuclides

This figure is a reproduction of Fig. 5 in Lindner and Turkevich (53). The dashed and dotted line shows the  $(\lceil n/\lceil f \rceil)$  values presented in Table 5-4, calculated from the estimates of fission competition in the present work.

Lindner and Turkevich (53)

---- Present work



 $\Gamma_n/\Gamma_f$  as a function of A for fissionable nuclides

## CHAPTER VI

## SUMMARY AND CONCLUSIONS

An experimental technique for the determination of absolute (p,xn) cross-sections on the natural alpha-emitter thorium-232 has been developed, which eliminates many of the experimental difficulties encountered in earlier work. It is not necessary with the present method to use stacked-foil techniques, nor is it necessary to perform chemical separations on the bombarded target. The method may be adaptable to measurements on other naturally alpha-active targets (e.g. lutetium, radium, actinium, protactinium and uranium). In the present measurement, which uses a very thin thorium target, traversed only once by an external proton beam, the energy spread is less than 2% FWHM. With the counting technique used, the <sup>232</sup>Th(p,6n)<sup>227</sup>Pa cross-sections were measured to within about 4%, and the  $^{232}$ Th(p,7n) $^{226}$ Pa cross-sections to within about 12%. This is the first such measurement on the latter reaction.

The excitation functions for both reactions show the characteristic shape expected for compound nucleus formation, and the high-energy tail due, presumably, to the prompt emission of one or more neutrons, followed by neutron evaporation. The <sup>232</sup>Th(p,6n) reaction has been measured in earlier experiments (6,7,8). The present experimental curves do not agree with the previous measurements, giving lower energies of the peak,

narrower peak widths, and different cross-sections. The earlier results are suspect, mainly because of the inevitable energy spread introduced in an internal beam technique using stacked foils.

The excitation functions have been analysed on the basis of a first approximation to the Jackson model (10) of neutron evaporation, in which we assume that the prominent peak is due mainly to delayed evaporation. A number of theoretical excitation functions were computed using different nuclear temperatures. In the <sup>232</sup>Th(p,6n)<sup>227</sup>Pa reaction a temperature of l.l MeV was selected to place the peak of the function at the position of the experimental peak, and the resulting curve (normalized to the same peak height as the experimental points) gave excellent shape agreement to the data. In the <sup>232</sup>Th(p,7n)<sup>226</sup>Pa reaction, a temperature of 1.3 MeV likewise predicts a theoretical curve which, when normalized, also gives excellent agreement to the shape of the experimental points. These temperatures do not agree with the higher values reported in previous work on similar heavy nuclei (1,6,7,8), but they are consistent with the results of more recent work on 127I (3). It is believed that the earlier estimates of level densities may be inaccurate, accounting in part for the discrepancy; also, the theoretical treatment of evaporation may well have to be modified to account for the "cooling" of the nucleus in the evaporation process.

The theoretical excitation functions for thorium are an order of magnitude higher than the experimental ones. It is shown that this is consistent with estimates of fission competition, and that values of the  $(\lceil n / \lceil r \rceil)$  ratios estimated in the present work agree well with earlier estimates (53).

#### APPENDIX I

## SAMPLE CROSS-SECTION CALCULATION

As a example, this calculation is for the absolute 232Th(p,6n) reaction cross-section using a proton beam of energy 47.44 MeV. Since secular equilibrium occurs, an alpharay of 8.00 MeV in the daughter nuclide 215At was observed instead of direct emission from the parent nuclide 227Pa. The parameters required in the equation (3-14) are given by:

a). Parameters which are not considered to contribute to statistical error:

t = 15 minutes

 $\lambda_{n} = 9.413 \times 10^{-17} \text{per min.}$ 

 $t_1 = 18$  minutes

 $2 = 1.809 \times 10^{-2}$  per min.

t<sub>2</sub>= 58 minutes

Y'= 100 %

 $S = 1.507 \text{ cm}^2$ 

Y = 100 %

Z'=100% (normalized absolute value)

Z = 84.15% (normalized absolute value)

b). Parameters subject to random error:

 $R_a = (2974 \pm 69)$  counts

 $P = (1.042\pm0.017)\times10^{13} \text{ protons}^*$ 

 $Q = (1.894 \pm 0.035)$  counts per min.

(\*= the error was obtained by averaging the counts of the scaler, fed by a standard pico-ampere source)

Thus, the cross section is given the following calculation, where the random error is calculated as the R.M.S. value of the individual contributions.

$$\sigma = \frac{\text{S t } \lambda \lambda_n \text{ Y' Z' } R_a}{\text{P Q Y Z } (1 - e^{-\lambda t}) e^{\lambda t} (e^{-\lambda t}1 - e^{-\lambda t}2)}$$

$$1.057 \times 15 \times 1.809 \times 10^{-2} \times 9.413 \times 10^{-17}$$

$$1.042 \times 10^{13} \times 1.894 \times 100 \times 84.15$$

$$x = \frac{100}{(1 - \exp(-1.809 \times 10^{-2} \times 15))}$$

$$x = \frac{100}{\exp(1.809 \times 10^{-2} \times 15)}$$

$$\frac{2974}{(-e \times p(-1.809 \times 10^{-2} \times 18) - e \times p(-1.809 \times 10^{-2} \times 58))}$$

$$= (41.57 \pm 1.41) \times 10^{-27} \text{ cm}^2$$

$$= (41.57 \pm 1.41) \text{ mb.}$$

#### APPENDIX II

## NATURAL ALPHA-EMISSIONS OF THORIUM

The natural thorium of the targets include lines from  $^{232}\mathrm{Th}$ ,  $^{230}\mathrm{Th}$ , and  $^{228}\mathrm{Th}$ . These isotopes occur in natural thorium in the ratios  $^{232}\mathrm{Th}$ ;  $^{232}\mathrm{Th}$ ;  $^{228}\mathrm{Th}$  =  $^{10}$ :  $^{5}\mathrm{xlo}^{4}$ :1.

In the present work, the half-life of thorium-232 and the natural thorium alpha-energy standards for energy calibrations were taken from Table AII-l and AII-2 respectively.

Table AII-1 Half-life data for thorium-232 (70 D)\*

Half-life	reference*
1.45 x 10 <sup>10</sup> years	56M
1.39 x 10 <sup>10</sup> years	56P
$1.42 \times 10^{10} \text{ years}$	56s
1.41 x 10 <sup>10</sup> years	60F
1.401x 10 <sup>10</sup> years	63L

Value adopted in this work = 1.40 x  $10^{10}$  years Unweighted average = 1.414 x  $10^{10}$  years (70D)\*

Weighted average value = 1.404 x 10<sup>10</sup> years (70D)\*

56M = R. L. Macklin, H. S. Pomerance, J. Nucl. Energy,  $\underline{2}$  (1956) 243

56P = E. Piccotto, S. Wilgain, Nuovo Cimento, 4 (1956) 1525

56S = F. E. Senftle, T. A. Farley, N. Lazar, Phys. Rev., <u>104</u> (1956)1629

60F = T. A. Farley, Can. Jour. Phys., 38 (1960) 1059

<sup>\* =</sup> reference:

63L = L. J. LeRoux, L. E. Flendenin, Natl. Conf. Nucl. Energy,
Application of Isotopes and Radiation, Pretoria, South
Africa, F. L. Warren, Ed., Atomic Energy Board, Pelindaba,
South Africa, p. 83 (1963)

70D = "Nuclear Data Table" editor: Katharin Way, Section A,
Vol. 8, No.1-2, (1970), page 153, Academic Press, New York

Table AII-2 Alpha-energy standards in thorium

		alpha-	anangu		
Source	half-li		) % bra	nching	reference*
232 <sub>Th</sub>	1.40 x 10 <sup>10</sup> y 4.011		,	? ?	5 <b>7</b> H
230 <sub>Th</sub>	8.0 x 10 <sup>4</sup>	у 4.68 4.61	40 . 75 75	76 24	67L
Parent source	Half- life	alpha- emittor	alpha- energy(MeV)	% branc from pa	======================================
232Th or 228Th	1.40x10 <sup>10</sup> y	228 <sub>Th</sub>	5.427 5.344	71 28	53A 57S
	1.910 y	224 <sub>Ra</sub>	5.684	94	62B
		212 <sub>Bi</sub>	6.0506 6.0890	25 10	61R 60R
	. •	220 <sub>Rn</sub>	6.288	100	62B
		216 <sub>Po</sub>	6.777	100	62B
		212 <sub>Po</sub>	8.7854	64 ======	61R

\*= reference:

53A = F. Asaro, S. G. Stephenes, Jr., and I. Perlman,
Phys. Rev., <u>92</u> (1953) 1495

57H = B. G. Harvey, H. G. Jackson, T. A. Eastwood, and G. C. Hanna, Can. Jour. Phys., <u>35</u> (1957) 258

61R = Albrech Rytz, Helv., Phys. Acta, 34 (1961) 960

62B = Geneviève Bastin-Scoffier, Compt. rend., <math>254 (1962) 3854

67L = C. M. Lederer, J. M. Hollander, and I. Perlman,
"Table of Isotopes" sixth edition, (1967)

John Wiley and Sons, Inc., New York

57S = F. S. Stephens, Jr., F. Asaro, and I. Perlman, Phys. Rev., <u>107</u> (1957) 1091

60R = Albrech Rytz, Compt. rend., 250 (1960) 3156

#### REFERENCES

- (1). R.E. Bell and H. M. Skarsgard, Can, Jour. Phys., 3/4 (1956) 745
- (2). T. M. Kavanagh, J. K. P. Lee, and W. T. Link, Can. Jour. Phys., <u>M2</u> (1964) 1429
- (3). R. E. Turcotte, M. Sc. Thesis, (1968), McGill University, (unpublished)
- (4). J. C-C. Chang, M. Sc. Thesis, (1970)

  McGill University, (unpublished)
- (5). H. A. Tewes, Phys. Rev., 98 (1955) 25
- (6). M. Lefort, G. N. Simonoff et X. Tarrago, Nucl. Phys., <u>25</u> (1961) 216
- (7). W. W. Meinke, G. C. Wick, and G. T. Seaborg, J. Inorg. Nucl. Chem., 3 (1956) 69
- (8). C. Brun and G. N. Simonoff, Le Jour. de Phys. et le Radium, 23 (1962) 12
- (9). M. Hussonnois, Jour. de Phys., 25 (1964) 747
- (10). J. D. Jackson, Can. Jour. Phys., 34 (1956) 767
- (11). J. M. Blatt and V. F. Weisskopf, "Theoretical Nuclear Physics", John Wiley and Sons, Inc., New York, (1952), Chapter VIII and IX.
- (12). M. A. Preston, "Physics of the Nucleus",
  Addison-Wesley Pub. Company, Inc., London, (1962),
  Part V.
- (13). R. Serber, Phys. Rev., 72 (1947) 1114

- (14). M. M. Shapiro, Phys. Rev., 90 (1953) 171
- (15). H. McManus, W. T. Sharp, and H. Gellman, Phys. Rev., 93 (1954) 924A
- (16). H. L. Bradt, and D. J. Tendam, Phys. Rev., 72 (1947) 1117
- (17). S. N. Ghoshal, Phys. Rev., 80 (1950) 939
- (18). J. W. Meadows, Phys. Rev., 91(1953) 885
- (19). K. Otozai, S. Kume, A. Mito, H. Okamura, and R. Tsujino, Nucl. Phys., 80 (1966) 335
- (20). N. T. Porile and S. Tanaka, Nucl. Phys., 43 (1963) 500
- (21). G. B. Saha, N. T. Porile and L. Yaffe, Phys. Rev., 144 (1966) 962
- (22). D. R. Sachdev, N. N. T. Porile and L. Yaffe, Can. Jour. Chem., 45 (1967) 1149
- (23). K. Chen, Z. Fraenke, G. Friedlander, J. R. Grover,

  J. M. Miller, and Y. Shimamoto, Phys. Rev., 166 (1968) 949
- (24). E. L. Kelly, (1950), UCRL-1044, (unpublished)
- (25). E. L. Kelly and E. Segre, Phys. Rev., 75 (1949) 999
- (26) W. John Jr., (1955), UCRL-3093, (unpublished)
- (27). C. G. Andre, J. R. Huizenga, J. F. Mech, W. J. Ramler, E. G. Rauh, and S. R. Rocklin, Phys. Rev., <u>101</u> (p956) 645
- (28). C. G. Andre, W. J. Ranler, E. G. Rauh, R. J. Thorn, and J. R. Huizenga, Phys. Rev., 93 (1954) 925
- (29). R. E. Bell, Phys. Rev. <u>95</u> (1954) 651
- (30). H. M. Skarsgard, Ph. D. Thesis, (1955)

  McGill University, (unpublished)

- (31). S. Hontzeas and L. Yaffe, Can. Jour. Chem., 41 (1963) 2914
- (32). R. Holub, Ph. D. Thesis, (1970)

  McGill University, (unpublished)
- (33). G. H. McCormick and B. L. Cohen, Phys. Rev., 96 (1954) 722
- (34). H. A. Tewes and R. A. James, Phys, Rev. 88 (1952) 860
- (35). Robert C. Weast, "Handbook of Chemistry and Physics."

  Page B-141 49<sup>th</sup> edition (1968-1969) The Chemical Rubber Co.,

  Cleveland, Ohio, U. S. A.
- (36). "Varian e-Gun Evaporation Source Instruction Manual 8M-400 84 (September 1967)
- (37). A. J. McPherson and D. G. Douglas, Rev. Sci. Inst., 20 (1945) 457
- (38). K. Sevier Jr., and W. Parker, Nucl. Inst. and Meth. 6 (1960) 218
- (39). M. Dc Crebs, W. Parker and K. Sevier, Jr., Nucl. Inst. and Meth., 7 (1960) 160
- (40). H. A. Anderson, Nucl. Inst. and Meth., 12 (1961) 111
- (41). M. Tatcher, Nucl. Inst. and Meth., 46 (1967) 171
- (42). D. G. Burke and J. C. Tippett,

  Nucl. Inst. and Meth., 63 (1968) 353
- (43). A. H. F. Muggleton, and F. A. Howe Nucl. Inst. and Meth., <u>28</u> (1964) 242
- (44). R. B. Moore, Foster Radiation Laboratory
  McGill University, (Private Communication)

- (45). C. F. Williamson, J-P. Boujot and J. Picard,
  "Table of Range and Stopping Power of Chemical Elements for Charged Particles of Energy 0.05 to 500 MeV"
  Report CEA-R 4042, (1966)
- (46). Ortec, Instruments of Research, Catalog No. 1000, 1001 and 1002
- (47). G. T. Carvey, W. J. Gerace, R. L. Jaffe, I. Talmi and I. Kellson, Rev. Mod. Phys., 41 (1961) S1, Supplement No. 4, Part II
- (48). K. J. Le Couteur, "Nuclear Reactions" Vol.1, page 318,
  North Holland (1959)
- (49). X. Tarrago, J. Physique Rad., 23 (1962) 1
- (50). C. M. Lederer, J. M. Hollander, and I. Perlman,
  "Table of Isotopes" sixth edition, (1967)

  John Wiley and Sons, Inc., New York
- (51). Y. Fujimoto and Y. Yamaguchi, Progr. Theoret. Phys. Japan, 5 (1960) 76
- (52). Robert Vandenbosch and Glenn T. Seaborg,
  Phys. Rev., <u>110</u> (1958) 507
- (53). Manfred Lindner and Anthony Turkevich, Phys. Rev., 119 (1958) 507
- (54). W. D. Myers and W. J. Swiatecki, UCRL Report 11980 (unpublished)
- (55). R. Vandenbosch and J. R. Huizenga, Proceedings of the Second United Nations International Conference on

Peaceful Uses of Atomic Energy, Geneva, 1958. (United Nations, Geneva, 1958), A/conf. 15/P/688

#### ACKNOWLEDGEMENTS

I wish sincerely to express my heartfelt appreciation to Dr. R. B. Moore and Dr. J. E. Crawford for their encouragement, illuminating discussions, and candid comments during the course of this work.

The present project on thorium was suggested and supervised by Dr. Moore, and the original ideas for the apparatus, experimental method, and basic experimental technique were largely due to discussions with him. I would like to thank him as well as for assistance in the programming of the PDP-15 computer, which was used to calculate the theoretical cross-sections.

Dr. J. E. Crawford has supervised me in the writing and revision of this thesis, and has particularly assisted in discussions of theoretical problems, including the background of the theory of fission competition.

I would also like to thank Dr. Moore, Dr. Crawford and Mr. D. Cheng for their assistance in cyclotron operation and in the bombardments.

Dr. Shun Hayakawa has also helped me in candid discussions of a number of problems during the course of this work.

This research was carried out with the financial assistance of the Atomic Energy Control Board of Canada.